AD-A162 663 INVESTIGATION INTO THE FATIGUE CRACK INITIATION PROCESS IN METALS..(U) ROCKWELL INTERNATIONAL THOUSAND OAKS CA SCIENCE CENTER F W MORRIS ET AL. DEC 85 SC5379.9FTD 1/1

UNCLASSIFIED N00C-87046-60 N62269-83-C-0267 F/G / NL

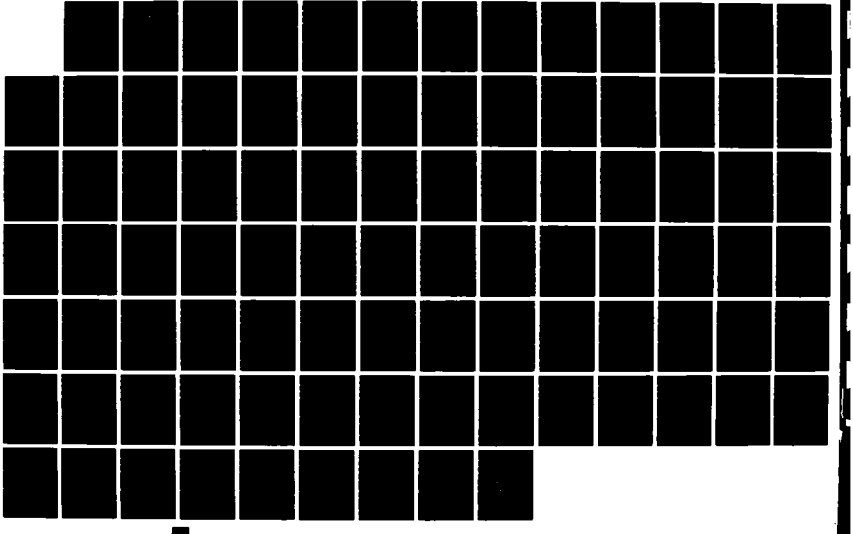

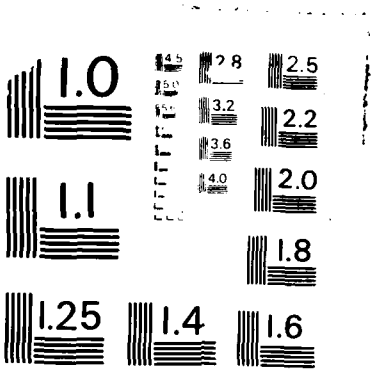

REPORT NO. NADC-87046-60

INVESTIGATION INTO THE FATIGUE CRACK INITIATION PROCESS IN METALS

W.L. Morris, B.N. Cox, M.R. James

Rockwell International
1049 Camino Dos Rios
Thousand Oaks, CA 91360

DECEMBER 1985

FINAL REPORT

Contract No. N62269-83-C-0267

Approved for Public Release; Distribution is Unlimited.

Prepared for
NAVAL AIR DEVELOPMENT CENTER
Department of the Navy
Warminster, PA 18974

NOTICES

REPORT NUMBERING SYSTEM – The numbering of technical project reports issued by the Naval Air Development Center is arranged for specific identification purposes. Each number consists of the Center acronym, the calendar year in which the number was assigned, the sequence number of the report within the specific calendar year, and the official 2-digit correspondence code of the Command Office or the Functional Department responsible for the report. For example: Report No. NADC-86015-70 indicates the fifteenth Center report for the year 1986 and prepared by the Systems and Software Technology Department. The numerical codes are as follows:

CODE	OFFICE OR DEPARTMENT
00	Commander, Naval Air Development Center
01	Technical Director, Naval Air Development Center
02	Comptroller
05	Computer Department
07	Planning Assessment Resources Department
10	Anti-Submarine Warfare Systems Department
20	Tactical Air Systems Department
30	Battle Force Systems Department
40	Communication & Navigation Technology Department
50	Mission Avionics Technology Department
60	Air Vehicle & Crew Systems Technology Department
70	Systems & Software Technology Department
80	Engineering Support Group

PRODUCT ENDORSEMENT – The discussion or instructions concerning commercial products herein do not constitute an endorsement by the Government nor do they convey or imply the license or right to use such products.

UNCLASSIFIED

SECURITY CLASSIFICATION OF THIS PAGE

REPORT DOCUMENTATION PAGE

1a REPORT SECURITY CLASSIFICATION Unclassified	1b RESTRICTIVE MARKINGS N/A
2a SECURITY CLASSIFICATION AUTHORITY	3 DISTRIBUTION/AVAILABILITY OF REPORT Approved for public release; distribution unlimited.
2b DECLASSIFICATION/DOWNGRADING SCHEDULE	
4 PERFORMING ORGANIZATION REPORT NUMBER(S) NADC-87046-60	5 MONITORING ORGANIZATION REPORT NUMBER(S) N/A
6a NAME OF PERFORMING ORGANIZATION Rockwell International Science Center 6b OFFICE SYMBOL (If applicable)	7a NAME OF MONITORING ORGANIZATION N/A
6c ADDRESS (City, State and ZIP Code) 1049 Camino Dos Rios Thousand Oaks, CA 91360	7b ADDRESS (City, State and ZIP Code) N/A
8a NAME OF FUNDING/SPONSORING ORGANIZATION Naval Air Development Center 8b OFFICE SYMBOL (If applicable)	9 PROCUREMENT INSTRUMENT IDENTIFICATION NUMBER Contract No. N62269-83-C-0267
8c ADDRESS (City, State and ZIP Code) Warminster, PA 18974	10 SOURCE OF FUNDING NOS PROGRAM ELEMENT NO / PROJECT NO / TASK NO / WORK UNIT NO
11 TITLE (Include Security Classification) INVESTIGATION INTO THE FATIGUE CRACK INITIATION PROCESS IN METALS (U)	
12 PERSONAL AUTHOR(S) Morris, W.L.; Cox, B.N.; James, M.R.	
13a TYPE OF REPORT Final 13b TIME COVERED FROM 08/03/83 TO 09/02/85	14 DATE OF REPORT (Yr, Mo, Day) DECEMBER 1985 15 PAGE COUNT 82
16 SUPPLEMENTARY NOTATION	
17 COSATI CODES FIELD / GROUP / SUB GR	18 SUBJECT TERMS (Continue on reverse if necessary and identify by block number) Fatigue, Crack Initiation, Deformation, Surface Properties, Microplasticity, Aluminum Alloys

19 ABSTRACT (Continue on reverse if necessary and identify by block number)

The foundation for a physically derived model of fatigue crack initiation in metals under spectrum loading is described. The work focuses on the microplastic deformation properties of a surface subject to stresses under the bulk elastic limit. A theoretical description of the highly localized plastic strains in individual surface grains, known to be pertinent to aluminum alloys, is developed with the support of high spacial resolution, high sensitivity strain measurements. These are made within individual grains of a Al 2219-T851 model material by a scanning electron microscopy technique. An important finding is that fatigue causes the local flow stresses in individual large surface grains to fall dramatically to less than 50% of their prefatigue values. The local stress-strain behavior is then controlled by the external load spectra, but is greatly influenced by the reaction stresses within a microplastic grain generated when its plasticity is constrained by the essentially elastic surface. Because of the constraint, the local stresses in a grain differ markedly from the applied. The theoretical models developed allow these stresses to be calculated and local mechanical properties of the surface including flow stress and

20 DISTRIBUTION AVAILABILITY OF ABSTRACT UNCLASSIFIED UNLIMITED ☒ SAME AS RPT ☐ DTIC USERS ☐	21 ABSTRACT SECURITY CLASSIFICATION Unclassified
22a NAME OF RESPONSIBLE INDIVIDUAL Dr. H.C. Tsai	22b TELEPHONE NUMBER (Include Area Code) 215-441-2871 22c OFFICE SYMBOL 6043

DD FORM 1473, 83 APR EDITION OF 1 JAN 73 IS OBSOLETE

UNCLASSIFIED

SECURITY CLASSIFICATION OF THIS PAGE

(Block 19 Continued)

plastic moduli to be estimated from experimental data.

An especially interesting anti-clockwise motion of the external stress-local strain hysteresis loop near grain boundaries is observed, and is explained by a simple dual-domain deformation model. It results from an inhomogeneity in mechanical properties with a higher flow stress within the grain near the boundary. Opportunities for the use of such deformation theories to predict crack initiation lifetime are discussed.

FORWARD

This program was made possible by techniques and associated equipment for the high spatial resolution measurement of microscopic strains in surfaces, developed as a research tool under Rockwell International IR&D support. The work was facilitated by a coordination with effort on a program under contract to NSF-DMR, which supplied important pieces of experimental data used to test the models of inhomogeneous surface deformation described herein. The program was sponsored by the Naval Air Development Center under the supervision of first Paul Kozel and then of Dr. H.C. Tsai. At the Rockwell Science Center, Fred (W.L.) Morris, Brian Cox and Mike James acted as co-investigators.

TABLE OF CONTENTS

TABLE OF CONTENTS (Continued)

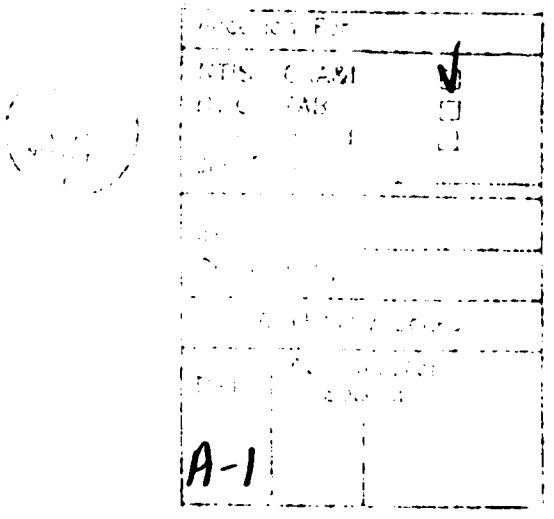

LIST OF FIGURES

LIST OF FIGURES (Continued)

LIST OF FIGURES (Continued)

1.0 INTRODUCTION AND BACKGROUND

Our long-range goal is to understand the micromechanics of fatigue crack initiation and to use this insight to construct a model of the stochastic variability of crack initiation under the spectrum loads pertinent to aircraft. We have focused our attention on situations where cracking is caused by peak loads below the alloy elastic limit. The genesis of the cracking is highly localized plastic deformation, usually in individual grains of an alloy and at its surface. Exciting and important discoveries about the mechanical properties of surfaces have been made by this research. These are essential ingredients in the mathematical description of the micromechanics of localized deformation, an area in which we have also made advances. This report documents the progress which has been made. The major effort has been to develop theoretical tools and models needed to extract the mechanical properties of the surfaces from experimentally measured local microplastic strains. These same models are the core of our representation of the micromechanical behavior of the surface and will be a starting place for any future formulation of a description of the overall stochastic behavior of crack initiation in the presence of surface deformation. A parallel program dealing with surface microplasticity has been supported by NSF.[1] Where pertinent, results from the NSF contract are also reported here with appropriate acknowledgement. As the NADC/NAVAIR research began, we relied upon the NSF experimental data to test the NAVAIR/NADC surface deformation models. Then, as this program advanced to spectrum loads, additional experimental data were obtained with the NAVAIR funding. The NSF research now involves 4% Cu-Al alloys.

The major findings of our research pertain to the alloy Al 2219-T851, the model material used in this study. However, there is reason to believe that our conclusions are generic to all high-strength structural aluminums, and have important implications to other structural materials, especially to certain steels. We have discovered that the flow stresses within the larger grains of 2219 decrease progressively with fatigue, ultimately falling to less than 30% of their prefatigue value. Usually, the surrounding surface remains

elastic. These changes occur slowly, and over short time intervals the deformation behaves as if the local flow stress was a constant. The effect of loading sequence on the mean stress within a microplastic grain is simply determined by the reaction stresses created when the plastic deformation is confined by the nearly elastic surrounding matrix. Herein is the apparent source of many load sequence effects on fatigue lifetime.

We begin our report by describing in detail the micromechanical models of the deformation of a surface which have been developed (Sec. 2). Their application to analysis of the mechanical properties of the surface of Al 2219-T851 is then described, and the implication of the models to the response of the alloy to selected load sequences is discussed (Sec. 4). Finally, we briefly discuss our findings in light of the opportunities for future research needed to develop an implementable initiation lifetime prediction methodology (Sects. 5 and 6).

2.0 DEFORMATION MODELS

Our theory and analysis of localized surface deformation comprises several elements. These are:

(i) The description of the constraints imposed upon a deformed grain by the surrounding elastic matrix;

(ii) treatment of the observed nonuniformity of the strain fields within a grain, especially the tendency of the center of the grain to become softer with fatigue relative to the boundary regions;

(iii) the modelling of observed hysteretic properties of the total strain as a function of the applied stress; and

(iv) the calculation of plastic work accrued in a grain during fatigue, for future correlation with the statistics of particle fracture as a test of the crack initiation modelling conjectures.

These theoretical considerations raise very complex questions, and involve many areas in which the available information is insufficient to decide with certainty what is the best or even a valid model. On many points, the experimental results reported in Sec. 4.0 are the only quantitative data available, representing the limit of guidance to theoretical modelling. Therefore, we have chosen to use the simplest approach possible at every stage, not diverting effort to details and exactitudes that are, in our best judgement, most likely ancillary to the determining physics. We have adopted a phenomenological approach, conjecturing a reasonable form for a given function, and then determining various parameters by direct comparison with the data. By this approach we have allowed the experimental results to speak for themselves as far as possible, rather than imposing *a priori* theoretical prejudices.

We shall begin in Sec. 2.1 by describing the theory of homogeneous deformation in a single grain. Expressions are derived for the plastic and total strains as a function of the applied load. These are used in Sec. 4.0 to deduce the flow stress and strain hardening parameter (or plastic stiffness constant) from experimental hysteresis loops. Various models for the yield stress and strain hardening are investigated. The models for the yield stress generally correspond to von Mises'[2] criterion, appearing in different forms depending on whether the local stress state is assumed to be uniaxial or biaxial. Strain hardening is treated either by Prager's kinematic hardening model,[3] or by a simplified hybrid model that allows certain memory effects in the local stress-strain response. We shall also describe application of these models to loading sequences consisting of one block at constant amplitude followed by another at reduced amplitude. It will be shown that experimentally observed memory effects manifest in the transient plastic response following the change in load amplitude, can help to determine the correct model for strain hardening.

A model of certain observed inhomogeneities in the strains in a grain will be introduced in Sec. 2.2. This model has been used (Sec. 4) to analyze surface strain data for Al 2219-T851, where the center and boundary regions of a typical, microplastic grain were found to have different plastic strains, and, by inference, different mechanical properties. This inhomogeneity is modeled by considering the grain boundary region to be a subdomain, homogeneous within itself, nested in the rest of the grain which is also homogeneous. This "dual domain" model is able to simulate an extraordinary, and experimentally observed, anticlockwise motion in the hysteresis loops of the measured total strain vs external stress. This phenomenon implies that the center of the grain suffers extreme softening during fatigue.

In Sec. 2.3, a generalization of the dual domain model is presented that deals with a biaxial stress state, which is the general case for a grain at a free surface. We believe that this model will be a powerful tool for studying not only the biaxial stress state, but also all kinds of hysteresis

effects. A computer code implementing the model has been completed. It is the means to an eventual understanding of damage accumulation, and the prototype of a functioning deformation model valid under all kinds of spectrum loading.

For various reasons, including the general state of theoretical opinion and the import of certain previously published results on particle fracture, the total plastic work done may be a good measure of the status of fatigue damage leading to initiation. Therefore, in Sec. 2.4 we discuss briefly the accumulation of plastic work in a homogeneous grain. We show how this would be readily included in the computer program for the dual domain model, and illustrate the importance of further careful studies of hysteresis and memory effects in deciding the aptness of assumed work hardening behaviors.

At the end of this section, we present a brief review (Sec. 2.5) of other various modelling approaches we have considered over the course of this program. Although none of these approaches is per se part of the set of models described in Secs. 2.1-2.4, they nevertheless provided decisive and valuable information at various stages of our learning process. Several of them remain outstanding candidates for more detailed theories in the future.

2.1 The Deformation of a Homogeneous Grain Under Uniaxial Stress

There are important cases where the inhomogeneity of a grain must be taken into account, as will be described later. However, in many experimental observations the grains apparently deform uniformly, and even in an inhomogeneous grain, most of its interior region may still be regarded as homogeneous. To analyze hysteresis data for all such cases, relationships between the plastic strain and the local and external stress were derived for a homogeneous grain.

The grain was assumed to be ellipsoidal and embedded in a wholly elastic matrix. The effect of the free surface (the specimen's surface) was neglected because of numerical demonstrations of its relative unimportance, as

described in Sec. 2.5. The material was assumed to be elastically isotropic, and Young's modulus E^e was taken to be uniform everywhere.

According to Eshelby,[4] if the plastic deformation in an ellipsoidal inclusion is homogeneous, then the internally constrained strain and stress are also homogeneous. In this sense, the assumption of homogeneity in the plastic strain is self-consistent, and one may easily write down the local stress in terms of the applied load and the state of plastic strain.

There is no evidence of strong slip bands in the measured strains nor of shearing deformation of the overall shape of the observed grains. Therefore, it is assumed that the plastic deformations are pure extensions or contractions in the frame of reference defined by the axes of the ellipsoid. In other words, the ellipsoidal axes coincide with the principal axes of the plastic strains. As illustrated by Fig. 2.1, we will consider one axis of symmetry the ellipsoidal grain to be parallel to the x-axis which is also the stress axis for the uniaxial external stress state. If we then write for the components of the plastic strain ε^p that

$$\frac{\varepsilon_y^p}{\varepsilon_x^p} = p \quad , \tag{1}$$

and

$$\frac{\varepsilon_z^p}{\varepsilon_x^p} = q \quad , \tag{2}$$

we may consider the state of plastic strain to be entirely defined by ε_x^p and the ratios p and q. The plastic strains are assumed to conserve volume, so that

$$1 + p + q = 0.$$

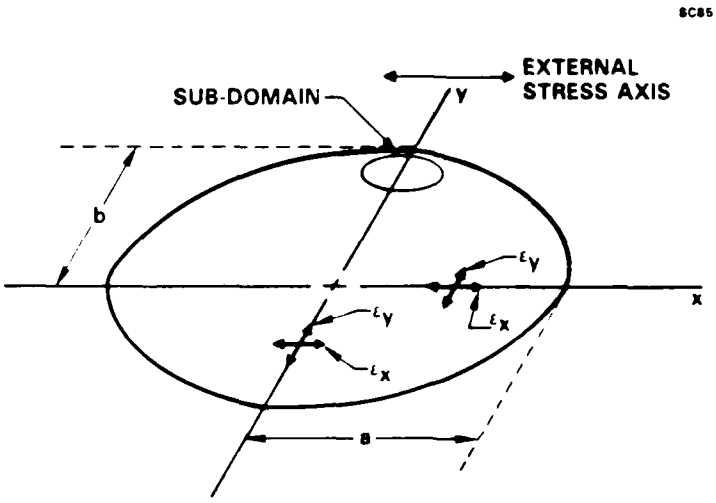

Fig. 2.1 Schematic illustration of a cross-section of the ellipsoidal grain, showing strain components. The x-axis is parallel to the external stress and z is taken to be normal to the surface.

The components of the local stress σ^{λ} may be written in terms of the applied stress σ^{a} and ε^{p}. In particular,

$$\sigma_x^{\lambda} = \sigma^a - \alpha E^e \varepsilon_x^p \tag{3}$$

where α is a function of p and q and depends on the shape of the grain. It is derived from Eshelby's tensor S_{ijkl}, which relates the total constrained strain to the unconstrained transformation strain in an ellipsoidal inclusion. Parameter α usually lies between 0.5 and 1 (see Sec. 2.2 for further discussion and Fig. 2.7).

2.1.1 Stress State

For the simplest models in which the stress state is always assumed to be approximately uniaxial, Eq. (3) is the only statement needed to establish the relationship between σ^{λ}, σ^{a} and ε^{p}. If the local stress is to be treated as biaxial, then the other components of σ^{λ} and ε^{p} must be consid-

ered. Discussion of the biaxial case is deferred to Sec. 2.3. We shall first consider in detail the behavior of models based on the assumption that the stress state is uniaxial. This turns out to be approximately correct even if the biaxial stress is included, and permits us to derive some very enlightening expressions for certain important characteristics of the observed hysteresis loops.

Even on the macroscopic scale, where experiments are much easier, there remains doubt and controversy over the best way to describe hysteresis effects arising from plastic flow under various load spectra. On the microscopic scale of the interior of a grain, no one knows the true state of affairs. We are presenting the first data on the subject. There is no current knowledge of the manner of strain hardening under monotonic or cyclic loads, the degree or existence of Bauschinger's effect, other memory effects in the shape of the yield locus, or the effects of fatigue. Therefore, our approach has been to apply simple models containing just three parameters to be determined by fitting to experimental data. These may be identified with a microplastic flow stress σ_0, a linear strain hardening parameter (or plastic stiffness) E^p, and α, which determines the reaction stress and depends upon grain shape. Limits on the range of α can be defined from the surface grain shape, but α also depend upon grain depth. However, caution must be used in assessing the physical significance of these parameters because their values are to a degree model-dependent. We will discuss this further later.

It is assumed, in the the uniaxial models, that the local stress and plastic strain are always linear functions of the applied stress. In the absence of incremental plastic strain, this is clearly valid. During plastic strain, it amounts to saying that the strain-hardening is linear, which results in the equilibrium hysteresis loop for the grain always being a parallelogram. By all our knowledge of macroscopic plasticity, this is a reasonable model capable of describing the experimentally observed loops. However, as we shall discuss in Sec. 2.5, the implications for studying the accumulation of plastic work during fatigue require careful thought.

2.1.2 Yield Conditions

Saint Venant[5] guessed the now established fact (generalized by Levy[6]) that increments in the components of plastic strain are proportional to the corresponding components of the deviatoric stress. In the deforming grain, we must, of course, consider the local stress. If this is uniaxial, then it follows that p and q of Eqs. (1) and (2) are always constant and equal to -1/2. Therefore, the factor α in Eq. (3) is also constant, and it also follows that the linear strain hardening conjecture may be expressed as

$$d\varepsilon_x^p = \frac{d\sigma_x^\ell}{E^p} \quad , \tag{4}$$

leading to the following expression for the increment in total strain in the plastic regime:

$$d\varepsilon_x^t = d\sigma_x^\ell \left(\frac{1}{E^e} + \frac{1}{E^p}\right) \quad . \tag{5}$$

If the material is not yielding, then

$$d\varepsilon_x^t = \frac{d\sigma_x^\ell}{E^e} \quad . \tag{6}$$

Equations (3)-(6) are immediately sufficient to determine the increments in plastic and total strain given an increment in the applied load. To determine the entire hysteresis loop, a yield criterion must be included to distinguish between the elastic and plastic regimes.

In the uniaxial case, the yield criterion of von Mises, that the second invariant of the deviatoric stress tensor reach a critical value, is simply

$$'J_2 = {}'\sigma_x^{\ell 2} + {}'\sigma_y^{\ell 2} + {}'\sigma_z^{\ell 2} = 6k^2$$

or

$$\sigma_x^{\ell} = \sqrt{3}\ k\ , \tag{7}$$

where primes appearing as prefixes denote a deviatoric quantity. The quantity $\sqrt{3}\ k$ is the yield stress under uniaxial tension, and we denote it σ_0 in our models. (However, as remarked above, σ_0 is strictly a parameter of the model, and must be interpreted carefully.)

The presence or absence of Bauschinger's effect is anticipated by considering two models of the way the yield point in one loading reversal is changed by the magnitude of the maximum plastic strain achieved during the prior loading reversal. One model, which we shall call the "stationary" model, assumes that σ_0 is unchanged by plastic strain. This is clearly valid only for fully reversed cyclical loading, but this is the case in all the experiments to be reported. This criterion may be written

$$d\sigma_x^{\ell} \cdot \sigma_x^{\ell} > 0$$

and

$$|\sigma_x^{\ell}| > \sigma_0 \tag{8}$$

where σ_0 is constant. In the "stationary" model, the only memory of prior loading (such as Bauschinger's effect), arises from the fact that the local stress in a grain is affected by the constraint of its plastic deformation. The other yielding model, which we shall call the "kinematic" model, is Prager's[3] model of kinematic hardening. Following plastic deformation during

one reversal, flow in the opposite direction in the next reversal always occurs when the magnitude of the local stress σ_x^ℓ changes by $2\sigma_0$ from its final value σ_i on the prior reversal. If $\eta = \pm 1$ denotes the sense of the current reversal, the "kinematic" criterion for yield is

$$\eta(\sigma_x^\ell - \sigma_i) > 2\,\sigma_0 \quad . \tag{9}$$

2.1.3 Equilibrium Loop Response

In fully reversed loading, the properties of these deformation models verifiable by experiment are easily discovered with some simple algebra. The experiments involve the measurement of total local strains (ε^t) or loop widths (W) vs the applied external stress σ^a. The following results neglect the biaxial stress components induced by the localized plastic deformation. Under fully reversed cyclic loading of constant amplitude, both yielding models predict that the total strain vs external load hysteresis will be a parallelogram. Since this should correspond to the observed hysteresis loop, we shall consider it in detail.

Let the maximum amplitude of the applied stress be s, and let the onset of yield during the loading half of a cycle occur when $\sigma^a = s_1$ (see Fig. 2.2). Then the characteristics of the hysteresis loop are as follows:

(a) "Stationary Model"

$$s_1 = \frac{2\sigma_0(E^p + \alpha E^e) - \alpha E^e s}{2E^p + \alpha E^e} = \sigma_0 + (\sigma_0 - s)\,\frac{\alpha E^e}{2E^p + \alpha E^e} \,. \tag{10}$$

$$s_1 < \sigma_0$$

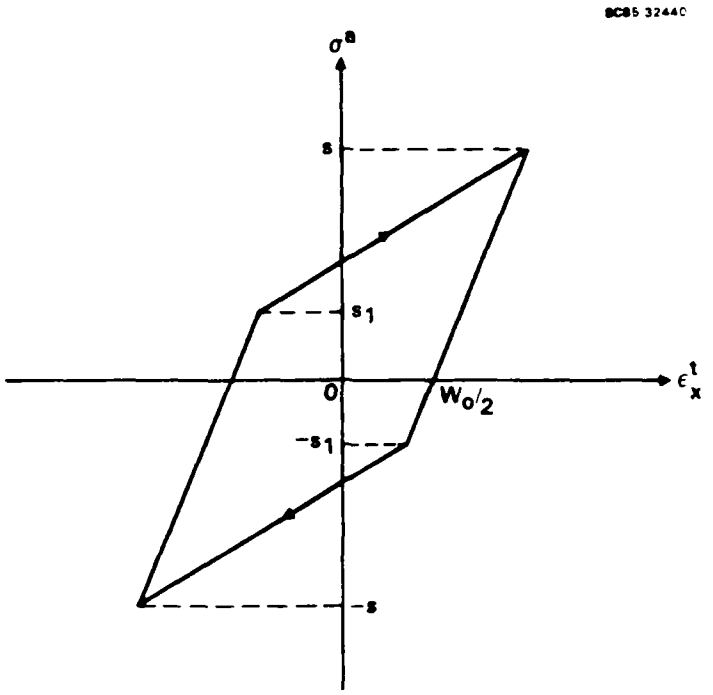

Fig. 2.2 Illustration of variables s, s_1 and W_0 in the analysis of hysteresis in a homogeneous grain. The subscript "o" on W_o indicates the loopwidth at $\sigma_a = 0$. W_o is the range in ϵ_t at $\sigma_a = 0$.

The maximum value ϵ^p_{max} of $|\epsilon^p_x|$ is

$$\epsilon^p_{max} = \frac{s - \sigma_0}{2E^p + \alpha E^e} \text{ , and} \tag{11}$$

the maximum value ϵ^t_{max} of $|\epsilon^t_x|$ is

$$\epsilon^t_{max} = \frac{s}{E^e} + (s - \sigma_o)\frac{(1 - \alpha)}{2E^p + \alpha E^e} = \frac{s}{E^e} + (1 - \alpha)\epsilon^p_{max} \text{ .} \tag{12}$$

The width W_0 of the loop when the externally applied stress is zero is shown as a function of σ_0 in Fig. 2.3a, and as a function of s in Fig. 2.3b. Figure 2.3a shows that, for fixed load amplitude the loop width first opens and then

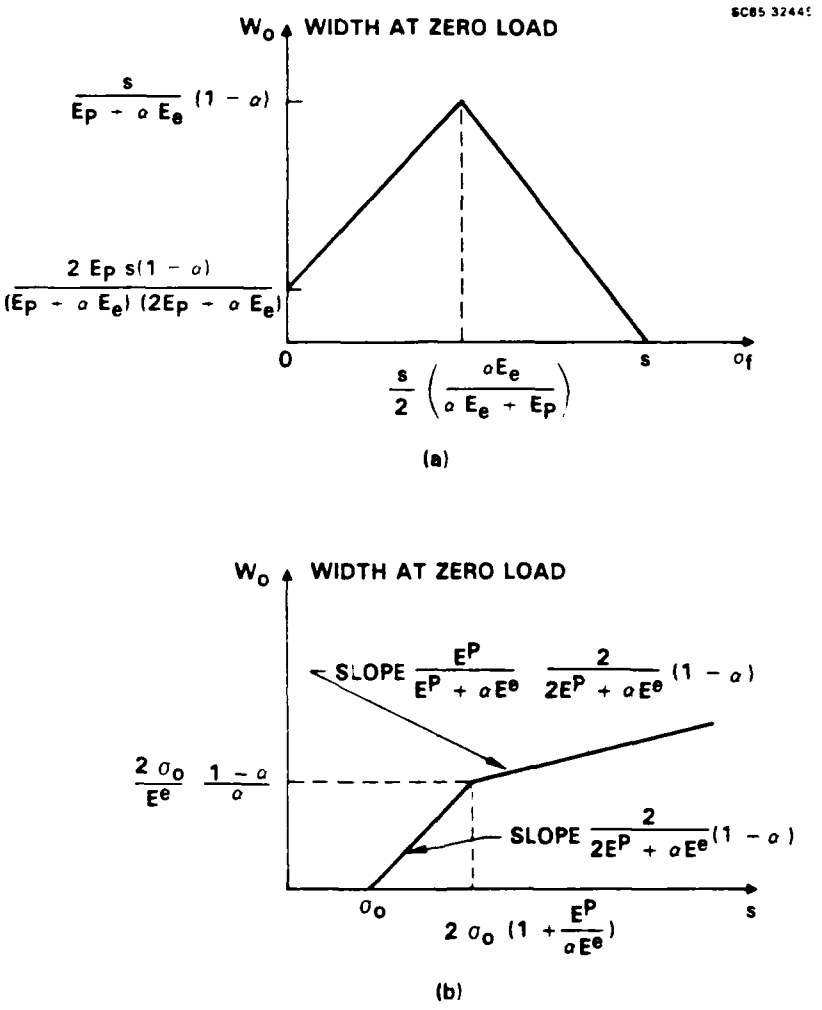

Fig. 2.3 The width of the hysteresis loop of total strain vs applied load at zero applied load for the "stationary" model, (a) vs σ_0 for constant s and E^P; (b) vs s at constant σ_0 and E^P.

closes again as the local flow stress falls from s to zero. The curve is symmetric about its peak, and passes through the origin if the material is elastic-perfectly plastic ($E^P = 0$). The reduction of W_0 for small σ_0 occurs simply because yield occurs before the external load returns to zero on each reversal; i.e., for $s_1 < 0$. On the other hand, the maximum plastic strain continues to increase as σ_0 decreases (Eq. (11)). Note that, since the maxi-

mum loop width at fixed load also varies inversely with the plastic stiffness E^p, an observed decrease in loop width may be attributed either to a falling yield stress σ_0 or a rising plastic stiffness E^p. Additional analysis to determine both E^p and σ_0 and the source of observed loop width closing is considered in Sec. 4.0. Figure 2.3b shows that, for fixed σ_0, the loop width is monotonically increasing with increasing cyclic stress amplitude. In the perfectly plastic case ($E^p = 0$), the loop width remains constant when the load exceeds $2\sigma_0$.

(b) "Kinematic Model"

$$s_1 = 2\sigma_0 - s. \tag{13}$$

$$\varepsilon^p_{max} = \frac{s - \sigma_0}{E^p + \alpha E^e} . \tag{14}$$

$$\varepsilon^t_{max} = \frac{s}{E^e} + (s - \sigma_0)\frac{1 - \alpha}{E^p + \alpha E^e} = \frac{s}{E^e} + (1 - \alpha)\varepsilon^p_{max} . \tag{15}$$

The width W_0 of the loop when the applied load is zero is shown as a function of σ_0 in Fig. 2.4a, and as a function of s in Fig. 2.4b. W_0 in the "kinematic" model does not decrease with falling flow stress, but remains constant when $\sigma_0 < 0.5$ s (Fig. 2.4a). For constant σ_0, W_0 is a strictly monotonically increasing function of s (Fig. 2.4b). Above $s = 2\sigma_0$, W_0 is a constant.

2.1.4 Transient Deformation Behavior

It is important to bear in mind that there is no sound a priori reason to prefer either the "stationary" or "kinematic" model. In fact, we should expect that the truth lies somewhere between them, i.e. that they may perhaps serve as limiting cases in the spectrum of plausible hardening models.

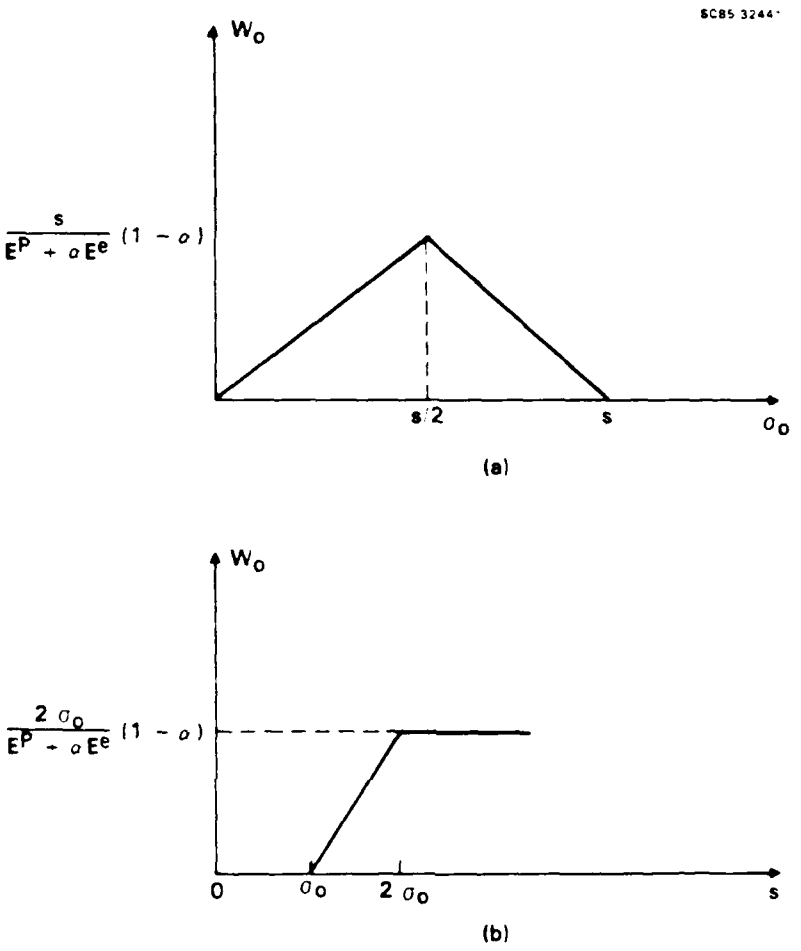

Fig. 2.1 The width of the hysteresis loop of applied load vs total strain at zero applied load for the "kinematic" model. (a) vs σ_0 at constant E^p. (b) vs s at constant E^p.

One of the essential differences between the two models is the presence or absence of memory effects. We shall now demonstrate this by considering a load sequence comprising a first block of fully reversed cycles at one constant amplitude s followed by another at a new, reduced amplitude s' that is still above the flow stress σ_0. We are interested in the existence and nature of any transient behavior at the beginning of the second loading block.

Consider first the "kinematic" model. The plastic strain at $s' > \sigma_0 > s_1$ when the load is increasing is

$$\varepsilon_x^p(s') = -\varepsilon_{max}^p + \frac{s' - s_1}{E^p + \alpha E^e}$$

$$= \frac{s' - \sigma_o}{E^p + \alpha E^e} \quad . \tag{16}$$

But, comparison with Eq. (14) shows that this is just the maximum strain that would be experienced in equilibrium if the load amplitude was s'. Therefore, when the load amplitude is reduced from s to s', the material at once follows the equilibrium loop for the new amplitude. No memory of the amplitude s or the existence of a prior higher amplitude block is present.

This is not the case for the "stationary" model. In the "stationary" model, the plastic strain at $s' > \sigma_0 > s_1$ is

$$\varepsilon_x^p(s') = -\frac{s - \sigma_0}{2E^p + \alpha E^e} + \frac{s - s'}{E^p + \alpha E^e}$$

$$= \frac{s' - \sigma_0}{2E^p + \alpha E^e} - \frac{E^p (s-s')}{(2E^p + \alpha E^e)(E^p + \alpha E^e)} \quad . \tag{17}$$

Comparison with the maximum plastic strain $\varepsilon_{max}^p(s')$ at equilibrium with a stress amplitude of s' (Eq. (11)) shows that $\varepsilon_x^p(s')$ is less than $\varepsilon_{max}^p(s')$ by the second term of Eq. (17). That is to say, at any point s' of the hysteresis loop, the deformation suffered on the prior cycle has not been sufficiently cancelled and reversed to be at the equilibrium level $\varepsilon_{max}^p(s')$ corresponding to s'. (The second term of Eq. (17) is always greater than or equal to zero. Equality occurs in the perfectly plastic limit $E^p = 0$.) If the new block at amplitude s' begins on a tensile reversal (see Fig. 2.5), then we may expect the following. The loop width measured between the first two zeroes of

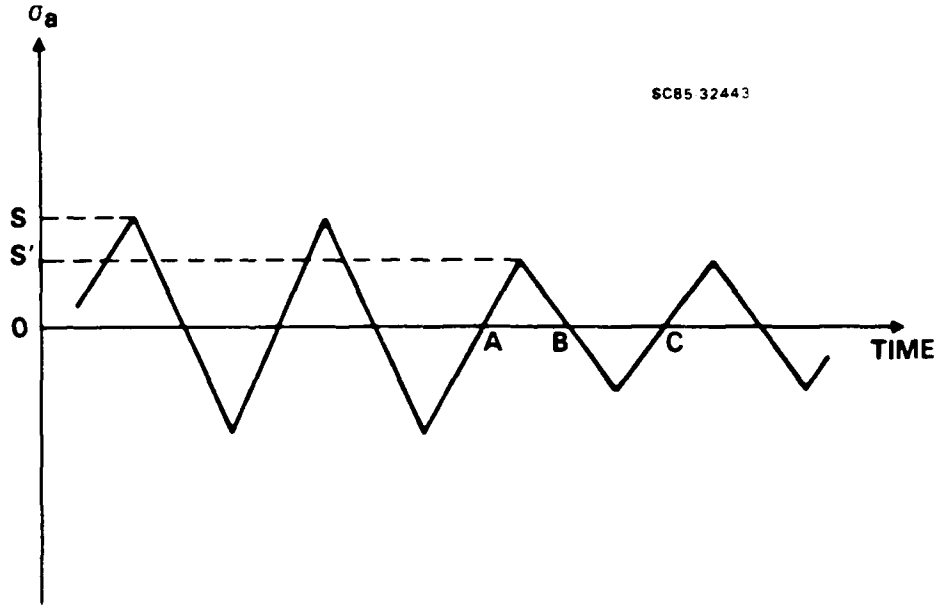

Fig. 2.5 Simulated loading history for the study of transient behavior.

the new block (points A and B in Fig. 2.5) will be greater than $W_0(s')$ for the equilibrium loop at load s'. If $s_1 > 0$, it is

$$W_0^A = W_0(s') + \frac{\alpha(1-\alpha)(s-s')}{(E^p + \alpha E^e)(2E^p + \alpha E^e)} \qquad (18)$$

The width measured over the compressive half cycle between the next two zeroes (points B and C) can be shown to be less than $W_0(s')$. The loop widths for succeeding reversals approach $W_0(s')$ asymptotically, and numerical examples show that the new equilibrium loop is achieved within about five cycles.

The fact that the "stationary" model shows memory in this transient region while the "kinematic" model does not will be used in the analysis of data (Sec. 4.0) to argue against Prager's purely kinematic hardening model. However, it should not then be inferred that the "stationary" model is therefore correct. In terms of the total strain vs local stress within a grain, the "stationary" model shows no Bauschinger effect, which may well lead to irreconcilable differences with other experiments. The truth probably lies

between these two extremes. One of the important tasks for future work is to devise measurements to test various strain hardening conjectures, under both uniaxial and biaxial stress states. This is a prerequisite to the development of a reliable model of microplastic deformation during stochastic loading.

2.2 Anomalous Hysteresis in Inhomogeneous Grains - The "Dual Domain" Model

For the sake of completeness, the following description of the dual domain model under uniaxial loading is presented. This model was formulated under the support of NSF funding when it became clear that a micromechanical approach we were trying (Sec. 2.5.3) as a means to derive quantitative values for σ_0 was not going to be fruitful. This analysis helps one visualize the underlying physics of the deformation which leads to the unusual grain boundary stress-strain response. However, the actual values of σ_0 found (Sec. 4.0) have been obtained by the numerical code developed for NADC/NAVAIR and discussed in Sec. 2.3, because the strain behavior when both domains are plastic can be extremely complex. Later it was realized that an even simpler assumption of homogeneous deformation could be profitable and this led to further analysis (Sec. 2.1) and data collection (Sec. 4.0), thus permitting calculation of σ_0, α and E^p from experimental data. This work and all the other theoretical results described here were developed under the NADC/NAVAIR contract.

One of the most extraordinary experimental phenomena observed in Al 2219-T851 is the existence of anticlockwise hysteresis in measurements of total strain as a function of external stress. That means, in some parts of a grain, the total strain on tensile loading can be greater than that at the same external stress during unloading. This corresponds to an anticlockwise motion about the hysteresis loop, rather than the normal clockwise motion. This anticlockwise motion is generally observed in a small region adjacent to the boundary of a microplastic grain, while the rest of the same grain exhibits the normal clockwise hysteresis. Continuing with the assumption that the local stress state is approximately uniaxial, we shall devise a simple model

that can reproduce all of the observed hysteresis phenomena. We then describe in Sec. 2.3 a generalization implemented on a computer to allow consideration of biaxial stress states and random loads.

In the "dual domain" model the inhomogeneity is introduced in the form of an ellipsoidal subdomain of the grain. As it turns out, with further approximations, the model's properties are shown to be independent of the precise position (but not the orientation) of the subdomain. However, we shall generally regard it as being at the grain boundary. Its axes are taken to lie parallel to those of the grain, but its shape, determined by the semi-axes, is not restricted.

Suppose that part of the grain lying outside the subdomain (call this domain 1) suffers a uniform deformation $\varepsilon_{ij}^{p}(1)$ and the subdomain (or domain 2) suffers a different uniform deformation $\varepsilon_{ij}^{p}(2)$. We may regard this state as the superposition of the deformation $\varepsilon_{ij}^{p}(1)$ acting over the entire grain and the deformation $\varepsilon_{ij}^{p}(2) - \varepsilon_{ij}^{p}(1)$ acting over the subdomain (domain 2). Because of the constraining matrix, reaction stresses accompany each of these deformations. As for the homogeneous grain, we require simple expressions for these reaction stresses in order to calculate the local stress.

Because of Eshelby's result,[4] we may, as for the homogeneous grain, consistently assume that as cyclic loading progresses, the subdomain (domain 2) will remain homogeneous. In the grain itself, the same would be true if not for the reaction field arising from and external to the deforming subdomain. The presence of this field implies nonuniformity of the local stress, and, therefore, of the plastic and total strains in the grain. However, if the subdomain is a small part of the entire grain, then except very close to subdomain boundaries, the reaction stress to subdomain deformation will be very small relative to the reaction stress created by the grain's own deformation. (We have reached this conclusion from many numerical calculations based on Eshelby's[7] expressions for the field outside an ellipsoidal inclusion.) Therefore, we neglect it. This amounts to assuming that the plastic deformation in the grain does not depend on the deformation in the subdomain,

a condition that happily simplifies the model's algebra. The local stress in the grain remains entirely determined by $\varepsilon_{ij}^{P}(1)$, as it was for the homogeneous grain. It is then consistent to assume that the grain (domain 1) also remains homogeneous throughout the fatigue process.

In an expanded notation in which the argument 1 refers to domain 1 and the argument 2 to domain 2, we now have that

$$\sigma_x^{\ell}(1) = \sigma^a - \alpha(1)E^e\varepsilon_x^P(1) \tag{19}$$

and

$$\sigma_x^{\ell}(2) = \sigma^a - \alpha(1)E^e\varepsilon_x^P(1) - \alpha(2)E^e(\varepsilon_x^P(2) - \varepsilon_x^P(1)) \ . \tag{20}$$

The coefficient $\alpha(2)$ is analogous to $\alpha(1)$, being derived from Eshelby's tensor S_{ijkl}, as described in Sec. 2.1. In the present section, we shall see that the relative values of $\alpha(1)$ and $\alpha(2)$, which depend on the shapes of the grain and the subdomain, have a controlling influence over the nature of hysteresis in the subdomain.

As in Sec. 2.1, we shall assume linear strain hardening, so that an equation of the form of Eq. (5) can be written for both domain 1 and domain 2. Young's modulus is assumed uniform everywhere, but the plastic stiffness E^P may be different in the two domains, so that, during plastic flow,

$$d\varepsilon_x^t(1) = d\sigma_x^{\ell}(1)\left(\frac{1}{E^e} + \frac{1}{E^P(1)}\right) \tag{21}$$

and

$$d\varepsilon_x^t(2) = d\sigma_x^{\ell}(2)\left(\frac{1}{E^e} + \frac{1}{E^P(2)}\right) \ . \tag{22}$$

To begin study of the "dual domain" model, the yield criterion of the "stationary" model of Sec. 2.1 will be assumed and flow stresses $\sigma_0(1)$ and $\sigma_0(2)$ will be attributed to the two domains. Results concerning the qualitative characteristics of hysteresis are unaffected by this choice of model for yielding.

Let us examine the conditions for anticlockwise hysteresis. Anticlockwise hysteresis occurs if, during the tensile loading part of the cycle, the slope of the external stress vs total strain curve after yielding exceeds that before yielding (see Fig. 2.6). In either domain, the slope S^e of the applied stress-total strain curve before yielding is E^e. In domain 1, the slope $S^p(1)$ after yielding, from Eqs. (19)-(22) is

$$S^p(1) = \left(\frac{E^p(1) + \alpha(1)E^e}{E^p(1) + E^e}\right) E^e \quad . \tag{23}$$

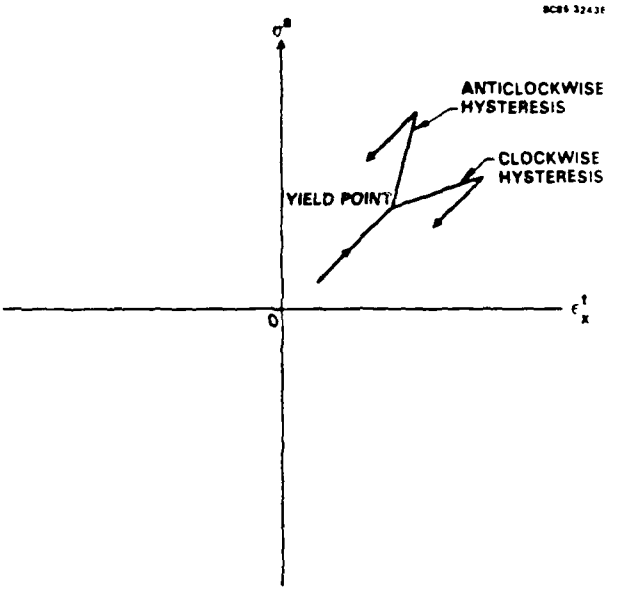

Fig. 2.6 Illustrating how anticlockwise hysteresis can occur.

In the subdomain, the slope $S^P(2)$ after yielding is

$$S^P(2) = \frac{(E^P(2) + \alpha(2)E^e)(E^P(1) + \alpha(1)E^e)}{(E^P(2) + E^e)(E^P(1) + \alpha(2)E^e)} E^e \quad . \tag{24}$$

For anticlockwise hysteresis to occur in domain 1, it can be seen from Eq. (23) that $\alpha(1)$ must exceed unity. The numerical results shown in Fig. 2.7 (obtained by following Eshelby's work[4]) show that α is rarely greater than 1 and can occur only for exceedingly flat grains (one transverse

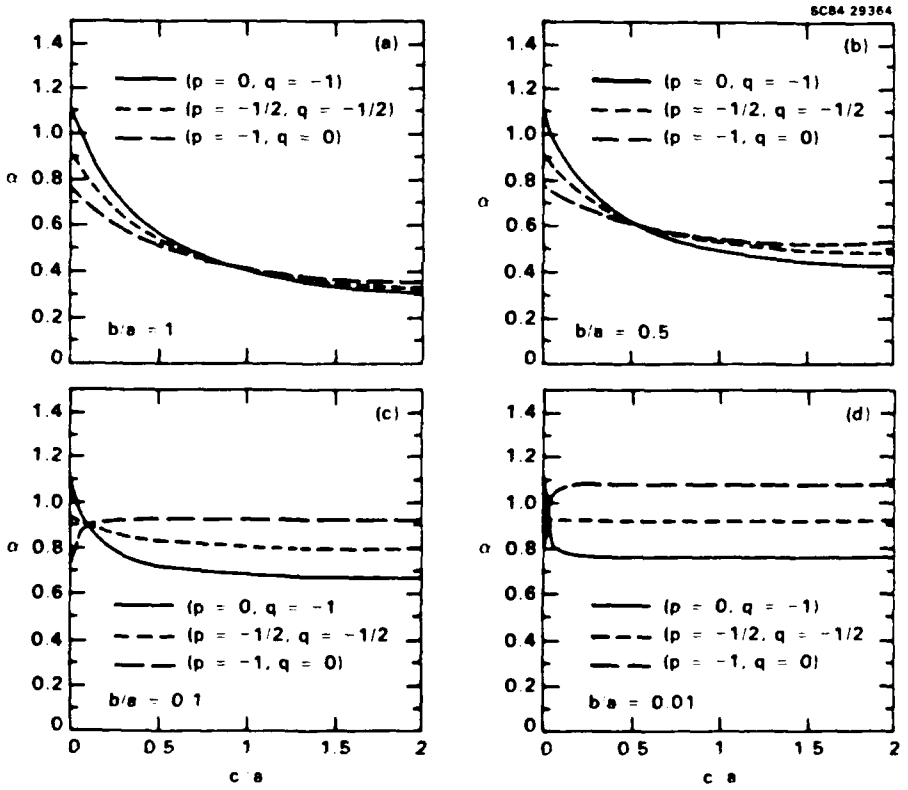

Fig. 2.7 Values of α determined by numerical implementation of Eshelby's equations for ratios of semiaxes of the grain dimensions (see Fig. 2.1). c is grain depth. From Ref. 1.

semi-axis less than a few percent of the other semi-axes). This is not believed to be the case in the experiments reported below. Furthermore, since α can barely exceed unity, the ratio of the slopes S^e to $S^P(1)$ can never equal that implied by the experimentally observed magnitudes of negative loop widths.

For anticlockwise hysteresis to occur in domain 2, $S^P(2)$ must exceed S^e. This may very easily happen. For example, when domain 2 is always elastic ($E^P(2) \to \infty$), as it sometimes appears nearly to be, the ratio of $S^P(2)$ to S^e is just

$$\frac{S^P(2)}{S^e} = \frac{E^P(1) + \alpha(1)E^e}{E^P(1) + \alpha(2)E^e} \quad . \tag{25}$$

This exceeds unity whenever $\alpha(1)$ exceeds $\alpha(2)$, and Fig. 2.7 shows that this is generally the case when domain 2 is more spherical than the entire grain. This situation is perfectly feasible. It is evident that anticlockwise hysteresis may also occur readily under similar conditions concerning the relative shapes of the domains, if $E^P(2)$ is finite. For any given $\alpha(1)$ and $\alpha(2)$, the condition may be stated as

$$\frac{E^P(2)}{E^P(1)} > \frac{(1 - \alpha(2))E^P(1) + (1 - \alpha(1))\alpha(2)E^e}{\alpha(1) - \alpha(2)} > 0 \quad . \tag{26}$$

For the usual case that $0 < \alpha(1) < 1$ and $0 < \alpha(2) < 1$, the numerator is positive, and we see that $\alpha(1)$ must exceed $\alpha(2)$ for a critical value of $E^P(2)$ to exist. Furthermore, when $0 < \alpha(1), \alpha(2) < 1$, the right hand side of Eq. (24) is a strictly monotonically increasing function of $E^P(2)$. Since it is also less than S^e when $E^P(2) = E^P(1)$, it follows that the critical value of $E^P(2)$, if it exists, is always greater than $E^P(1)$; i.e., the subdomain must be relatively hard for anticlockwise hysteresis to occur.

Note that no reference has been made yet to the flow stresses $\sigma_0(1)$ and $\sigma_0(2)$, except the implicit assumption that the local stresses have exceeded them at some point. The criterion for negative loop width is entirely determined by the plastic stiffness parameters and the shapes of the domains. The flow stresses $\sigma_0(1)$ and $\sigma_0(2)$ appear in the expressions for the magnitude of the loop widths. Furthermore, in the event that both domain 1 and then domain 2 yield on each reversal, the flow stresses determine the topology of the hysteresis loop. An example is illustrated schematically in Fig. 2.8. The point A marks the onset of yield in domain 1 during the tensile loading half-cycle. Between A and B, domain 2 remains elastic, and if $\alpha(1) > \alpha(2)$, the slope of the curve increases as shown in the figure. B marks the onset of yielding in domain 2 and, if $E^p(2)$ is less than the threshold given in Eq. (26), the slope of the stress-strain curve will become less than it was when both domains were elastic. This is the case shown. When the half-cycle is completed and unloading begins, the material response will descend on a line parallel to the original elastic loading line. However, depending on whether the load reversal occurs at C or C', the descending elastic line may or may not intersect the loading segment AB. Which case occurs depends on the rela-

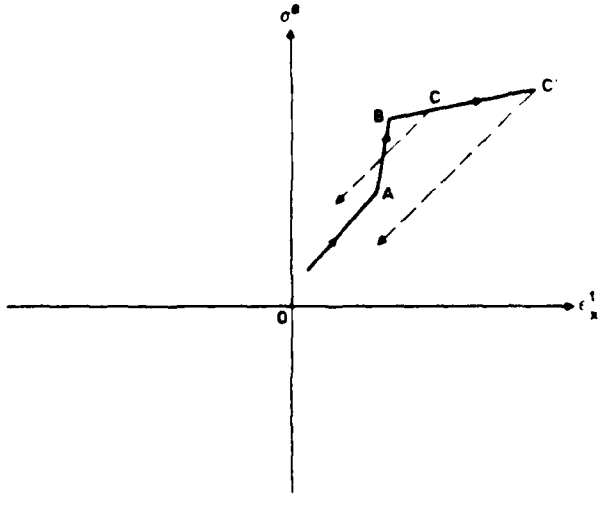

Fig. 2.8 Possible topologies for the hysteresis loop in a relatively hard subdomain.

tive magnitudes of $\sigma_0(1)$, $\sigma_0(2)$, the load amplitude, as well as upon the plastic stiffnesses $E^P(1)$ and $E^P(2)$. For the loop ABC, the width measured at equal external stress during loading and unloading will appear positive (conventional) at high stresses and negative (anticlockwise) at low stresses. Observations of such patterns have indeed been made and are reported in Sec. 4.0.

In fact, as will be seen in Sec. 4.0 the "dual domain" model has a very high degree of success in explaining the first available measurements of strain inhomogeneity. Not only are the qualitative observations accounted for but even the values of the model's parameters giving best fit to the data look very plausible and, where applicable, are in good agreement with the values deduced from the much more reliable modelling of the deformation in homogeneous grains. However, one must be wary of being seduced by this success into inferring too much. Other assumed geometrical distributions of inhomogeneity may give equally appealing results, and we do not yet have enough data to know whether another model would be more or less realistic. Furthermore, we have not yet begun to investigate how the various observed hysteresis effects depend on the nature of the stress state. It could easily be that an analysis of inhomogeneity in a biaxial stress field will reveal qualitatively different mechanisms for generating anticlockwise hysteresis. In the next subsection, we shall present a model, already implemented on a computer, to tackle just such questions.

2.3 The "Dual Domain" Model in the Biaxial Case

The "dual domain" model has been generalized to consider the generally biaxial stress state that exists in a grain at a free surface. Since there is no longer a direct proportionality between increments in the components of plastic strain and an increment in the applied load, it is no longer possible to derive simple expressions for the characteristics of hysteresis as in the preceding subsections. Instead, we have developed a numerical

approach, for which a computer program has now been written. Since it will be the basis of future work on the subject, we shall describe it here fully.

In the numerical model, the status of the system is defined at any time by the applied stress and the x and y principal components of plastic strain in each domain (the free surface being the plane z = 0). Given an increment $\delta\sigma^a$ in the still uniaxial applied stress, the change in local stress state is given by

$$\delta\sigma_x^{\ell}(1) = \delta\sigma_x^a - \alpha_x \delta\varepsilon_x^p(1)$$

$$\delta\sigma_y^{\ell}(1) = \alpha_y \delta\varepsilon_x^p(1)$$

$$\delta\sigma_x^{\ell}(2) = \delta\sigma_x^{\ell} - \alpha_x'' \delta\varepsilon_x^p(2) - \alpha_x' \delta\varepsilon_x^p(1)$$

$$\delta\sigma_y^{\ell}(2) = \delta\sigma_y^{\ell} + \alpha_y'' \delta\varepsilon_x^p(2) + \alpha_y' \delta\varepsilon_x^p(1) \quad . \tag{27}$$

It is to be remembered that coefficients α_x, α_x', α_x'', α_y, α_y', and α_y'' depend not only on the grain's shape, but also on the components of the deviatoric local stress tensor. They are derived, as before, from Eshelby's tensor S_{ijkl}. However, since the ratios of the components of the deviatoric stress tensor are always changing (in contradistinction to the uniaxial case) the coefficients must be evaluated afresh at every increment of load.

The increments in plastic strain are assumed to be given by the Prandl-Reuss equations:[8,9]

$$\delta\varepsilon_x^P(1) = \frac{3'\sigma_x^{\ell}(1)}{2E^P(1)} \cdot \frac{d\bar{\sigma}^{\ell}(1)}{\bar{\sigma}^{\ell}(1)}$$

$$\delta\varepsilon_y^P(1) = \frac{3'\sigma_y^{\ell}(1)}{2E^P(1)} \cdot \frac{d\bar{\sigma}^{\ell}(1)}{\bar{\sigma}^{\ell}(1)}$$

$$\delta\varepsilon_x^P(2) = \frac{3'\sigma_x^{\ell}(2)}{2E^P(2)} \cdot \frac{d\bar{\sigma}^{\ell}(2)}{\bar{\sigma}^{\ell}(2)}$$

$$\delta\varepsilon_y^P(2) = \frac{3'\sigma_y^{\ell}(2)}{2E^P(2)} \cdot \frac{d\bar{\sigma}^{\ell}(2)}{\bar{\sigma}^{\ell}(2)} \qquad (28)$$

where a preceding prime refers to a deviatoric quantity, and

$$\frac{d\bar{\sigma}^{\ell}(i)}{\bar{\sigma}^{\ell}(i)} = \frac{(2\sigma_x^{\ell}(i) - \sigma_y^{\ell}(i))\delta\sigma_x^{\ell}(i) + (2\sigma_y^{\ell}(i) - \sigma_x^{\ell}(i))\delta\sigma_y^{\ell}(i)}{(\sigma_x^{\ell}(i) - \sigma_y^{\ell}(i))^2 + (\sigma_x^{\ell}(i))^2 + (\sigma_y^{\ell}(i))^2} . \qquad (29)$$

From Eqs. (27) and (28) one has at once explicit expressions for the plastic strain increments $\delta\varepsilon_x^P(1)$ and $\delta\varepsilon_x^P(2)$ in terms of $\delta\sigma^a$, which may be regarded as simultaneous ordinary differential equations of the first order. They may be solved quite adequately by simple, low order techniques. In fact, a first order method has been used satisfactorily.

To begin, we have coded Prager's kinematic hardening rule for the translation of the yield locus in $(\sigma_x^{\ell}(i), \sigma_y^{\ell}(i))$ space in each domain. With von Mises criterion, the yield locus for domain i is given by

$$(\sigma_x^{\ell}(i) - \sigma_x^0(i))^2 - (\sigma_x^{\ell}(i) - \sigma_x^0(i))(\sigma_y^{\ell}(i) - \sigma_y^0(i)) + (\sigma_y^{\ell}(i) - \sigma_y^0(i))^2 = c_0^2$$

(29)

where $(\sigma_x^0(i),\ \sigma_y^0(i))$ defines the origin of the yield locus at any time, as given by Prager's pin and rigid frame model.[3] During yielding, if the local stress changes by $(\delta\sigma_x^\ell(i),\ \delta\sigma_y^\ell(i))$ in $(\sigma_x^\ell(i),\ \sigma_y^\ell(i))$ space, then, according to Prager's model, the translation $(\delta\sigma_x^0(i),\ \delta\sigma_y^0(i))$ of the origin of the yield locus is given by

$$\delta\sigma_x^0(i) = 1/D\ (\tilde{\sigma}_y^\ell(i) - 2\tilde{\sigma}_x^\ell(i))^2\ \delta\sigma_x^\ell(i) + (\tilde{\sigma}_x^\ell(i) - 2\tilde{\sigma}_y^\ell(i))(\tilde{\sigma}_y^\ell(i) - 2\tilde{\sigma}_x^\ell(i))\delta\sigma_y^\ell(i)$$

$$\delta\sigma_y^0(i) = 1/D\ (\tilde{\sigma}_y^\ell(i) - 2\tilde{\sigma}_x^\ell(i))(\tilde{\sigma}_x^\ell(i) - 2\tilde{\sigma}_y^\ell(i))\delta\sigma_x^\ell(i) + (\tilde{\sigma}_x^\ell(i) - 2\tilde{\sigma}_y^\ell(i))^2\ \delta\sigma_y^\ell(i)$$

where $D = (\tilde{\sigma}_y^\ell(i) - 2\tilde{\sigma}_x^\ell(i))^2 + (\tilde{\sigma}_x^\ell(i) - 2\tilde{\sigma}_y^\ell(i))^2$

and $\tilde{\sigma}_j^\ell(i) = \sigma_j^\ell(i) - \sigma_j^0(i)$. (30)

When using Prager's model, the origins $(\sigma_x^0(i),\ \sigma_y^0(i))$ should be regarded as independent variables constituting part of the status of the system at any time.

As with the uniaxial approximation, one finds that the kinematic model just defined contains no memory. If block loading is simulated, the system falls into its new equilibrium hysteresis loop on the first cycle of a new block. As we have already said, this contradicts experimental results presented below. Therefore, a necessary improvement of the computer simulation will be to include a better representation of strain hardening and Bauschinger's effect than Prager's kinematic model.

In its present form, the chief benefit of the computer program is that it allows rapid simulation of the plastic response to a biaxial local stress state. Furthermore, there is no restriction whatever on the uniaxial

applied load. This may follow any designated spectrum, since the load sequence is simply defined as a sequence of reversals of any amplitude. Because of the simplicity of the model, it would be quite feasible to follow many thousands of reversals in detail. Thus, the program gives us a powerful tool to study the role of accumulated plastic strain or total plastic work done in determining initiation rates under diverse loading histories. A phenomenological and testable distinction is drawn between such quantities in the interior of a grain and near its boundaries.

2.4 Plastic Work Done

For a given local stress σ^{ℓ} and a given plastic strain ε^{P}, the total irrecoverable plastic work done is

$$W^{P} = \int \sigma^{\ell}_{ij} \, d\varepsilon^{P}_{ij} \, . \tag{31}$$

Since there is good reason to expect plastic work to be a useful measure of fatigue damage, we shall consider now some simple expressions for the work done in a homogeneous grain under constant amplitude loading, using the "stationary" and "kinematic" uniaxial models described above (Sec. 2.1). The purpose of this exercise is to get a feeling for the effect upon the plastic work done for each model assumed for the yield criterion.

In the "stationary" model, the plastic work done in a single cycle of amplitude $s > \sigma_0$ is

$$W^{P}_{s} = \frac{2(s - \sigma_0)}{(2E^{P} + \quad E^{e})^2} \left[(E^{P} + \alpha E^{e})\sigma_0 + \quad E^{P} s\right] , \tag{32}$$

where the notation is as it was in Sec. 2.1. Since flow stress σ_0 will be shown to change with fatigue, it is interesting to consider W^p as a function of σ_0, as shown in Fig. 2.9. Also shown in Fig. 2.9 is the same function in the "kinematic" model, where

$$W_k^p = \frac{2\sigma_0(s - \sigma_0)}{E^p + \alpha E^e} . \tag{33}$$

Note that W_s^p and W_k^p always have the same maximum value, although it generally occurs at different values of the flow stress. When $E^p = 0$ (the perfectly plastic limit), W_s^p and W_k^p are identical. Note that if the flow stress were to fall from a high value near the applied load to nearly zero during fatigue, the rate of accumulation of plastic work will rise and then fall. This is just another manifestation of the opening and closing of the hysteresis loop under the same conditions noted in Sec. 2.1.

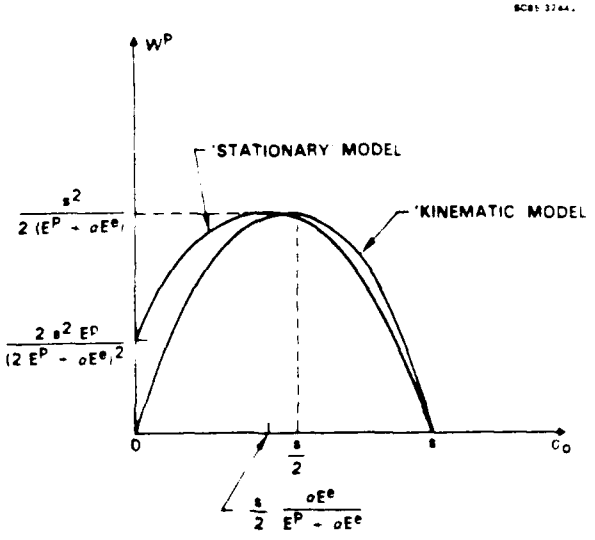

Fig. 2.9 The plastic work done in a homogeneous grain in one cycle during equilibrium hysteresis in the "stationary" and "kinematic" models as a function of flow stress σ_0.

From the interpretation of data, it can also be conjectured that plastic stiffness E^P changes with fatigue. Therefore W_s^P and W_k^P are plotted in Fig. 2.10 as a function of E^P. There are potentially important qualitative differences between the two models. In the "kinematic" model a simple inverse relationship exists. In the "stationary" model, the shape of the function depends on the values of the applied cycle stress amplitude s and flow stress σ_0. If $s = 2\sigma_0$, the W_s^P function is different from W_k^P only by a numerical factor. However, if $2\sigma_0 < s \leq 3\sigma_0$, a point of inflection is present in W_s^P, and if $s > 3\sigma_0$, a maximum exists at $E^P > 0$.

The conclusion to be drawn from this brief comparison is that even during constant amplitude loading, if the plastic stiffness is not constant, it is important (for the purpose of calculating plastic work done) to establish a good model for the yield criterion.

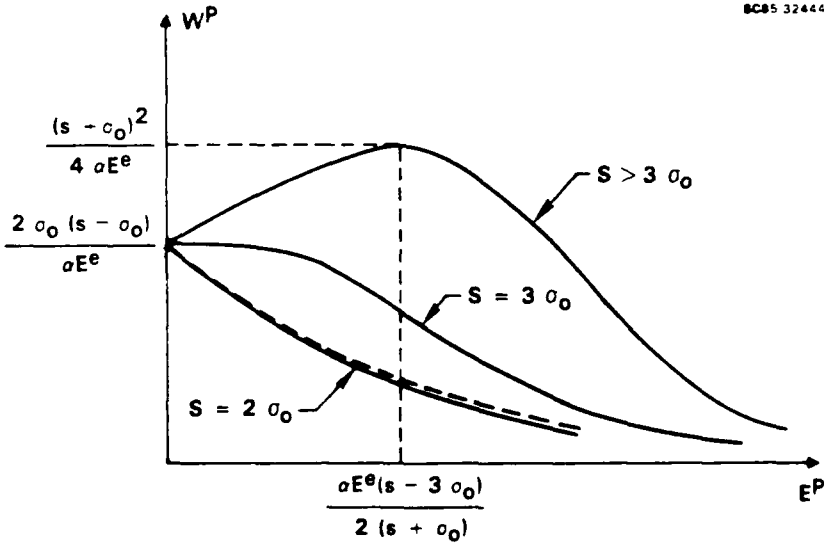

Fig. 2.10 The plastic work done in a homogeneous grain in one cycle during equilibrium hysteresis in the "stationary" (solid lines) and "kinematic" models (dashes) as a function of plastic stiffness or work-hardening parameter.

The addition of a plastic work calculation based on Eq. (31) to the computer program for the biaxial case is trivial. Because of the structure of the program, W^P would then be calculable for any assumed loading sequence. One possible means of testing a model for yielding is then to compare computer simulations for different loading sequences to see if the predicted accumulation of plastic work can be correlated with experimental observations (e.g., initiation events) that are expected to be sensitive to plastic work.

2.5 Other Associated Problems Studied

During the life of this program, several substantial tasks were undertaken that have not been presented as part of the deformation models in the preceding sections. Nevertheless, the information gleaned from these various studies remains an essential part of the rationale of our current models. Furthermore, some of the approaches that we discontinued (usually because of time limitations) remain viable and interesting ideas for future work. We shall therefore discuss them here briefly before moving on to report the experimental work and its analysis.

2.5.1 The Linear Chain Model

At the beginning of the program, the extent of interaction between two neighboring or close deforming grains was unknown. To examine this question, a crude linear model of interacting grains was formulated. A linear chain was chosen to represent the two-dimensional surface of the specimen in the belief that the important mutual interactions under uniaxial loading were felt only between grains lying in close proximity.

The mechanism for interaction between different grains was assumed to be the change in local stress in one grain caused by the elastic constraint field generated by the deformation in the other. This field was calculated by assuming that each grain was ellipsoidal and homogeneously deformed, and by invoking Eshelby's[7] solution for the field outside an ellipsoidal inclusion. Coding this solution on a computer constituted the major part of the work on

this model. The change in local stress in a grain because of reaction to its own deformation was, as in the extant model described in Secs. 2.1 to 2.4, calculated from Eshelby's[4] simpler solution for the field inside an inclusion.

The outcome of the chain model was moderately surprising but now believed by us, in the light of much more experimental data, to be clearly the case. The model showed that, as long as the plastic deformation in any grain is volume conserving, which is assuredly the case to a high degree of precision, then the change in local stress in even a neighboring grain is rather small. In fact, compared to the reaction to the grain's own deformation, it is essentially always neglible. Therefore, it became clear that most of the experimental data could and ought to be interpreted by assuming that each grain behaves independently of its neighbors, as though embedded in an entirely elastic matrix. This is a key premise of all of the models presented above. The coding of Eshelby's solutions for deformation outside the plastic grains later proved to be essential in the experimental verification of this hypothesis based upon a comparison of measured and predicted strains just outside of a deformed grain.

It should be stated, however, that there must be circumstances in which the model breaks down for an isolated deforming grain. If the coherence of the grain boundary fails, or if slip bands penetrate into a neighboring grain, or if plastic deformation begins to occur equally over groups of grains or even the whole surface, then a new model is needed. In such cases, a more realistic model than the crude linear chain model would also be required.

2.5.2 Corrections Due to the Free Surface

The reason that so many interesting results are so readily obtained from the models described above for deformation in a single grain, is essentially that great simplicity is afforded by being able to assume consistently that the deformation remains homogeneous. However, this is strictly correct only if the grain is an entire ellipsoid embedded in an infinite matrix. In our case, we have been modelling approximately semi-ellipsoidal grains at a

free surface of the specimen. It was therefore essential to examine closely the effects of the presence of the free surface, and to this end the following numerical work was carried out.

It was assumed that the deformation in the grain consists solely of pure extensions and pure contractions in the axis system defined by the grain's own axes. A free surface in a plane of symmetry of the grain can then be created by cancelling the normal tractions found across that plane in the solution of the constrained entire ellipsoid in an infinite space (see Fig. 2.11). The changes to the stress field at any point on the surface (or below it, if required) due to this cancellation can be found by integrating Mindlin's[10] Green's function for the half-space. This procedure was followed numerically by writing a computer program.

To calculate changes in the in-plane stresses σ_x and σ_y (where the free surface is the plane $z = 0$), one must evaluate the integral

$$\int (-\sigma_z) \frac{1 - 2\nu}{2\pi} \frac{x^2 - y^2}{(x^2 + y^2)^2} \, dxdy \qquad (34)$$

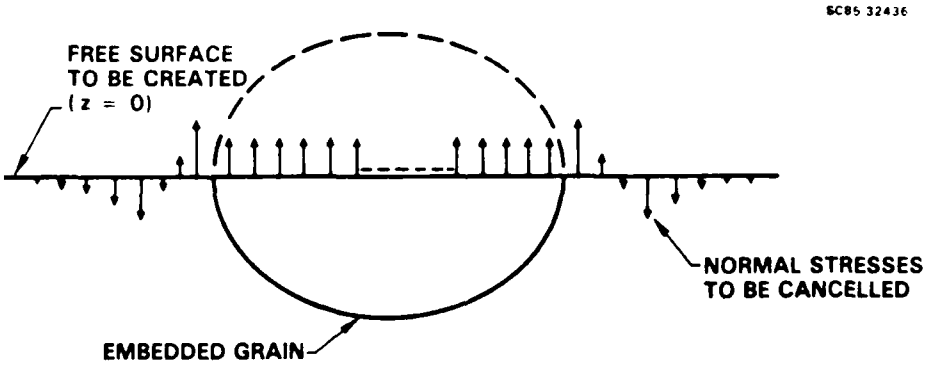

Fig. 2.11 The cancellation of normal tractions at the surface $z = 0$ to form a free surface.

where σ_z is the normal stress to be cancelled at the point (x,y) and the origin lies at the point where the correction is required. Quantity ν is Poisson's ratio. The singular nature of Eq. (34), together with the fact that σ_z generally suffers large, rapid changes just outside the ellipsoid, make the numerical task quite difficult. Nevertheless, in the short time available, sufficiently accurate solutions were obtained to reach some important conclusions.

The changes in the components of the in-plane surface stresses accompanying the creation of the free surface show a singularity at the grain boundary. This is the dominant feature of the example shown in Fig. 2.12. Analytical work on the surface displacements under another contract has proven that the accompanying singularity in the derivative of the normal displacement is logarithmic, and the implied weakness of the divergence is borne out by the

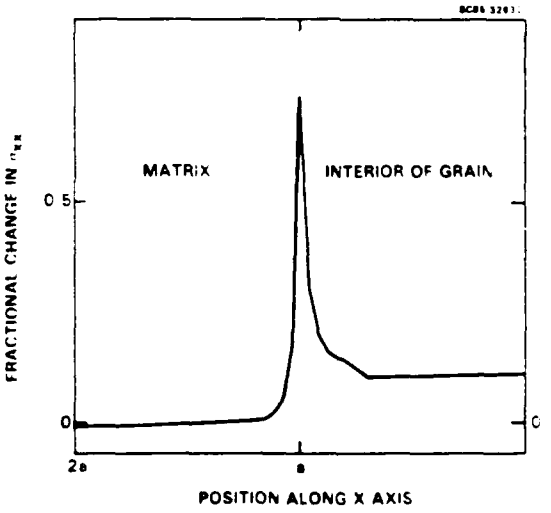

Fig. 2.12 An example of the change in σ_x along the applied stress axis due to the creation of the free surface. For a volume conserving deformation in the uniaxial model, normalized to the value of σ_x inside the entire ellipsoid before the creation of the free surface. Note a certain amount of numerical noise. a = 200 μm, b = 100 μm and c = 50 μm. There is a logarithmic singularity at the boundary which is averaged in the numerical procedure. This will be relaxed by localized plasticity.

numerical results, which show that it is very limited in range. The other feature of Fig. 2.12 is the magnitude of the stress corrections, which have been normalized against the internally constrained stress calculated for the entire homogeneous ellipsoid. They are very small, even quite close to the grain boundary. This has always been found to be the case if the plastic deformation in the ellipsoid was volume conserving. If it was not volume conserving, then the corrections were found to be quite substantial, typically ranging up to 0.3 on the normalized scale.

Since plastic deformations are indeed volume conserving, we proceeded to ignore the free surface effects in our modelling. However, an accurate analysis of strains, especially in the important grain boundary region, will probably require their inclusion. We are now in a good position to pursue this aspect in the future, because of the development of the numerical solutions.

2.5.3 Micromechanical Considerations

There are two levels on which the deformation measurements can be studied, differing in the physical scale at which attention is directed. The models presented above belong to the "macroscopic" scale in the sense that we have treated the material as possessing idealized, smoothly varying constitutive properties without consideration of the processes on a much finer, "microscopic" scale that lead to them. On the microscopic scale, in this context, are dislocations, slip bands, dislocation cells, and pile-ups. A feasible alternative approach to interpreting the experiments is to start on the microscopic scale in the first place, building up to the calculation of measurable macroscopic strains.

This kind of approach has been used in the past by many other workers. One application of particular interest is that of Tanaka and Mura[11] in their calculation of ratcheting plastic strains in a deforming grain. In this work, Muskhelishvili's solution[12] for the singular integral equation

governing the dislocation density in a one-dimensional pile-up is used. In such an equation, the dislocations experience mutual interactions, usually taken from the elastic solution to the field around a dislocation line in an infinite medium. These interactions sum to produce a back stress, which corresponds, on the macroscopic scale, to the reaction stress in a constrained inclusion calculated by Eshelby's technique (as described, for example, in Sec. 2.1). In either case, the back stress or reaction stress acts against further plastic deformation.

We have investigated the feasibility of solving a two-dimensional system of interacting dislocations to model deformation in a grain. A singular integral equation in two-dimensions was written with piece-wise continuous boundary conditions at the grain boundary to distinguish segments that were intact (diverging dislocation density) and segments where the boundary had failed and separated (vanishing dislocation density). Analytical solutions to such a problem are not known, but standard numerical techniques have been used on analogous problems in fluid mechanics with great success. Therefore, this approach should be considered viable, and the solution obtained would form a very valuable link between micromechanical concepts and the phenomenological constitutive relations used in studies on the macroscopic scale. We spent some time considering our options for implementation of such a model because success would allow the representation of deformation associated with grain boundary triple points, the interaction with internal grain deformation and better insight into the progression of fatigue-induced changes in flow stress. We concluded that while the opportunity was there, we did not have time to pursue this line further in this program. To take it to a useful conclusion would have been a major project in itself.

3.0 MATERIALS AND EXPERIMENTAL PROCEDURES

3.1 Materials

The Al 2219-T851 alloy has been used extensively in prior studies of crack initiation and short crack growth. Pertinent properties of the material are its cyclic yield strength of 360 MPa and mean longitudinal and short transverse grain diameters of 60 and 20 μm, respectively. The material has the highest as-received hydrogen content that we have encountered, and is therefore more microplastic than the average 2219 alloy. Specimens were fatigued in a dry nitrogen atmosphere to further magnify the microplastic strains achieved (see Ref. 13). Miniature tapered cantilever beam specimens were used[14] and were fatigued in fully reversed bending at ±85% of the yield strength. Prior to fatigue, the surfaces were prepared by a careful machining and polishing schedule involving use of progressively finer cuts then progressively finer polishing grits, ending with an 0.03 μm MgO powder. The residual surface stresses left by this procedure and measured by x-ray diffraction are small, ±4 MPa. After fatigue, localized strain measurements were made vs applied surface stress for values less than or equal to the maximum stress incurred during fatigue, using a bending jig in our SEM (see Ref. 13).

3.2 Measurements

The strain measurement procedures are described elsewhere,[13,15] but their essential features follow. The major impediment to accurate strain measurements using a SEM is its magnification stability, which is 2% in our instrument. This constraint would give a $\pm 2 \times 10^{-2}$ strain measurement sensitivity limit and is improved by placing a floating reference or microscopic ruler on the surface and gauging strains in the surface relative to the ruler. The measurement involves comparing micrographs of the ruler edges relative to the surface taken before and after deformation. We use thin mica flakes, which are held electrostatically to the surface. Prior to fatigue, these are placed into position within a grain using a micro-manipulator. Mica flakes

can be prepared which lie flat on the substrate and are sufficiently thin that the flake and substrate are co-focal at magnifications of 3×10^4. To avoid small parallax errors from substrate tilting under bending, all measurements in a particular sequence are taken at the same applied surface stress. Displacement data are obtained from micrographs of the before and after deformation conditions using a stereoimaging technique.[13,15] Before and after deformation pairs are viewed stereoscopically, and small in-plane relative displacements appear as height differences between the mica gauge and the surface. A photometric flying spot is used to convert the three-dimensional image into linear displacement data. We chose this rather complex data reduction technique because of its sensitivity. The human eye processes an entire segment of the flake edge image while making the displacement determination. This greatly reduces statistical errors. Furthermore, because the comparisons involve only the translation of an edge, which is nearly identical in both micrographs, the displacement measurement sensitivity is better than the SEM point-to-point resolution. By keeping surface contamination low through turbo pumping our SEM, differential displacement accuracies of ±30Å have been regularly achieved. In analysis of the displacement data to obtain strains, it can be shown that only the differential components of the x or y displacement need be considered in calculating the principal strains provided that local rigid body rotations which accompany the deformation are less that 1°. No examples where this limit have been exceeded were found in our study.

4.0 ANALYSIS OF EXPERIMENTAL DATA

Our experiments all involve the fatigue of Al 2219-T851, at stress amplitudes less than or equal to ±85% of the alloy bulk cyclic yield strength. Regions of substantial plastic deformation of the surface are found only in grains larger than 120 μm. So the plastically active grains have at least double the average grain size. Apparently, the early evolution of microplasticity with fatigue is confined within these grains, which act as isolated regions of plasticity constrained by an external matrix of smaller and essentially elastic grains. With continued fatigue, however, some of the largest microplastic grain sites show deformation which extends beyond their boundaries into the smaller neighbors. This characteristic is especially apparent at the longitudinal boundary site, relative to the stress axis, as indicated in Fig. 2.1. With extended fatigue, cracks form at such longitudinal boundary sites, but in 2219, it is the earlier rupture of constitutent particles within the grains which usually leads to the crack initiation important to lifetime.

As far as possible, we have restricted our study to grains whose deformation can be analyzed using the models of Sec. 2.0. These are grains whose surface cross-section is crudely elliptical, with their major axis parallel to the loading axis. When looking at deformation at the grain boundaries, we have avoided locations near triple points and sought transverse sites with boundaries nearly parallel to the external stress and longitudinal sites with boundaries nearly perpendicular to the external stress axis. Where appropriate to the analysis, the assumption that the deformation within a microplastic grain was uniform has been made in obtaining local values of flow stress from the experimental data.

This limitation appears to be acceptable as long as the grain interior is substantially softer than its surroundings. The dual domain deformation model is applied to estimate flow stresses near the grain boundaries. Over small numbers of cycles the local flow stresses within the plastically active grains appear to be quasi-static. Within the time frame of a short

loading segment, load sequence effects apparently arise from a coupling between the mean stress in the grain and the reaction stress to constraint of its deformation defined by the load sequence. Over longer fatigue segments, progressive changes in the local flow stress must be considered. The following analysis deals with four topics.

1. Flow Stress at Grain Interiors - The flow stresses are examined relatively early in fatigue using a uniform stationary deformation model, and applied to grains where the deformation is apparently confined to the grain interior.

2. Flow Stresses Near Grain Boundaries - The dual domain model is used to characterize flow stress variations within grains with emphasis on differences between sites in the interior and near the boundaries. [These results utilize NSF data, but the flow stresses come from numerical calculation done by the NADC/NAVAIR code described in Sec. 2.3.]

3. Flow Stress Evolution - This subsection presents what is now known about the progressive changes in local flow stress with fatigue, including the plastic disruption of grain boundaries.

4. Load Sequence Effects - The response of local strain ranges within microplastic grains to sudden changes in external load are examined.

4.1 Flow Stresses at Grain Interiors

First we examine some properties of the uniform deformation of an ellipsoidal grain by considering the stationary deformation model. An important result is that the experimentally observed width of the stress (external) vs strain (local) hysteresis loop in the grain is much less than the actual total plastic strain ε^{p}_{max} experienced over a loading cycle. The example (Fig.

4.1) is for fully reversed loading with s = 305 MPa. The loop width W_o is measured at zero external load (i.e., $\sigma^a = 0$), and ε^p_{max} is the plastic strain range encountered from minimum to maximum load in the cycle. Figure 4.2 makes the meaning of these two quantities a little clearer. The stress range in the stress (local) vs strain (local) loop in Fig. 4.2 is smaller because of the reaction stress caused by constraint of the grain's microplasticity. If yielding in tension is at a positive stress, then ε^p_{max} is just the width of the stress (local) vs strain (local) loop at σ (local) = 0. Notice in Fig. 4.1 that the measurable W_o reaches a maximum. This happens when yielding occurs at $\sigma^a = 0$. We are interested in this behavior for its

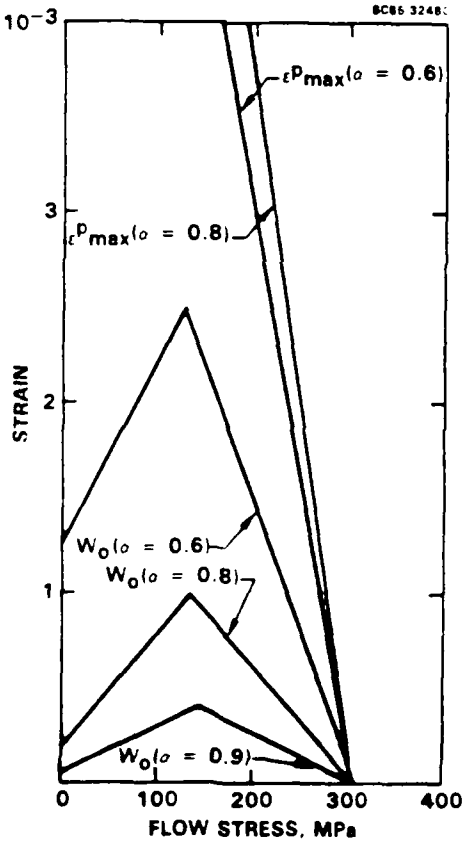

Fig. 4.1 Numerical values of loop widths and plastic strain range obtained with the uniaxial stationary homogeneous deformation model for s = 305 MPa and for several values of α.

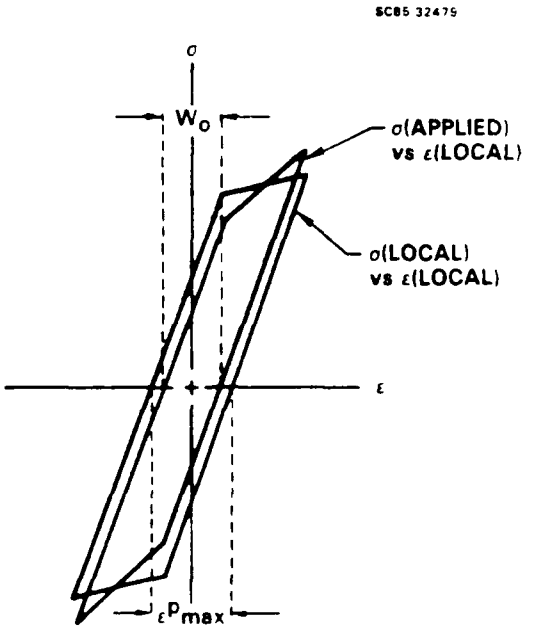

Fig. 4.2 Stress-strain response as experienced inside a grain σ (local) and as apparent to an experimenter σ^a (applied).

experimental implications and also because of its pertinence to crack initiation models. If hysteretic energy is the driving force for initiation, then W_o is the important loop parameter, while a plastic damage model would suggest description by ε^p_{max}.

The example in Fig. 4.1 has been constructed for an elastic-perfectly plastic material (i.e., $E^p = 0$). If we assume that yielding is controlled by a von Mises criterion, then $p = q = -1/2$ and Fig. 2.7 tells us that the common range of α values for our Al 2219 alloy will be 0.75-0.95, with $\alpha \approx 0.8$ being the most typical value. The reaction stress parameter α depends upon grain shape and we arrived at these numbers by assuming that the grain depth is quite shallow. Typical grain depths for the material under study are 10 to 20 μm. For such values of α the maximum observable loop widths for a microplastic grain in an elastic aluminum matrix at $\sigma^a = \pm$ 305 MPa should be $W_o \approx 1 \times 10^{-3}$. Indeed, this is approximately the experimentally observed maximum, suggesting that E^p during microplastic deformation may be quite small.

Clearly, however, we require a more direct determination of α and E^P to obtain the flow stress σ_0 from our experimental data. By a judicious choice of load sequence experiments, the measurements outlined in Fig. 4.3 can accomplish this analysis giving α, E^P and σ_0 for a "stationary" deformation model assumption. The measurement begins by fatiguing the material at a constant stress amplitude (s) to establish a quasi-static value of σ_0 in a grain. Two sets of W_0 loop widths are then measured at $\sigma^a = 0$, and involve characterization of W_0 resulting from fatigue at $\pm$ s', where s' $\leq$ s. If W_0 is measured for the first tensile loop to s' (case I in Fig. 4.3), then the stationary model predicts

$$W_0(1) = \left\{ s' - \sigma_0 + \frac{\alpha E^e (s - \sigma_0)}{2E^P + \alpha E^e} \right\} \frac{(1 - \alpha)}{E^P + \alpha E^e} \qquad (4.1)$$

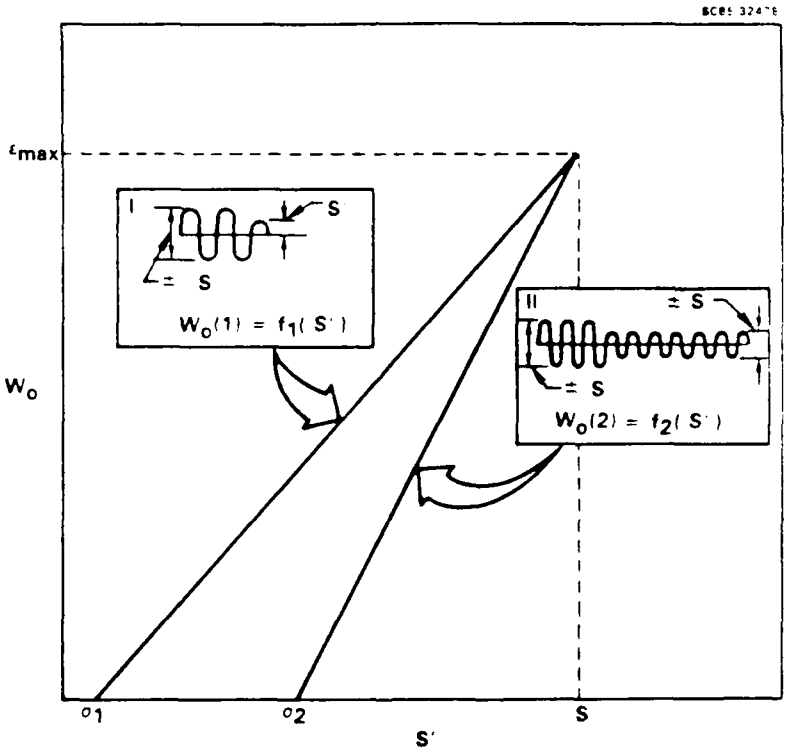

Fig. 4.3 Illustration of load sequence experimental used to obtain α, E^P and σ_0, based upon a "stationary" model analysis.

If the loop opening for fatigue at ± s' is allowed to return to equilibrium after the stress has been dropped from s (Case II in Fig. 4.3), then

$$W_o(2) = \frac{2(s' - \sigma_o)(1 - \alpha)}{2E^p + \alpha E^e} . \tag{4.2}$$

Relative to the intercepts σ_1, σ_2 and ε_{max} defined in Fig. 4.3, α, E^p and σ_o are obtained from Eqs. (4.1) and (4.2) and are simply:

$$\sigma_0 = \sigma_2, \tag{4.3}$$

$$\alpha = \frac{2(\sigma_o - \sigma_1)}{2(\sigma_o - \sigma_1) + \varepsilon_{max} E^e} , \tag{4.4}$$

$$E^p = \frac{(s - \sigma_o)(1 - \alpha)}{\varepsilon_{max}} - \frac{\alpha E^e}{2} . \tag{4.5}$$

Also, for $s' < \sigma_1$, $W_o(1) = 0$, and for $s' < \sigma_2$, $W_o(2) = 0$. Equations (4.3 - 4.5) must be rewritten if the quantity, s_1, defined in 2.1.3, is less than 0, in which case $\sigma_1 = 0$.

4.1.1 Analysis of Load Sequence Data

Six to eight values of loop widths must be measured to obtain sufficient accuracy to calculate E^p, α, and σ_o for a grain, using Eqs. (4.3)-(4.5). We have taken two such data sets for fatigue at s of approximately ± 300 MPa; one set is for a 330 μm grain after 500 cycles (Fig. 4.4); the other for a 120 μm grain after 10^4 cycles (Fig. 4.5). Both measurements were taken near the center of the grain parallel to the x or stress axis and over gauge lengths in excess of 100 μm. Please notice that the strain scale is an order of magnitude more sensitive for the 120 μm grain. The strains in this grain were tiny. Results of our analysis of these data using Eqs. (4.3-4.5) are given in Table 1.

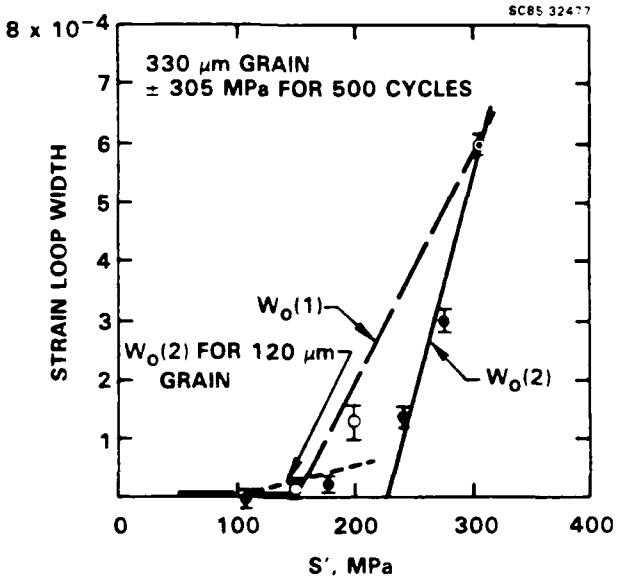

Fig. 4.4 Loop width vs s' for a 330 μm grain for load sequences (1) and (2).

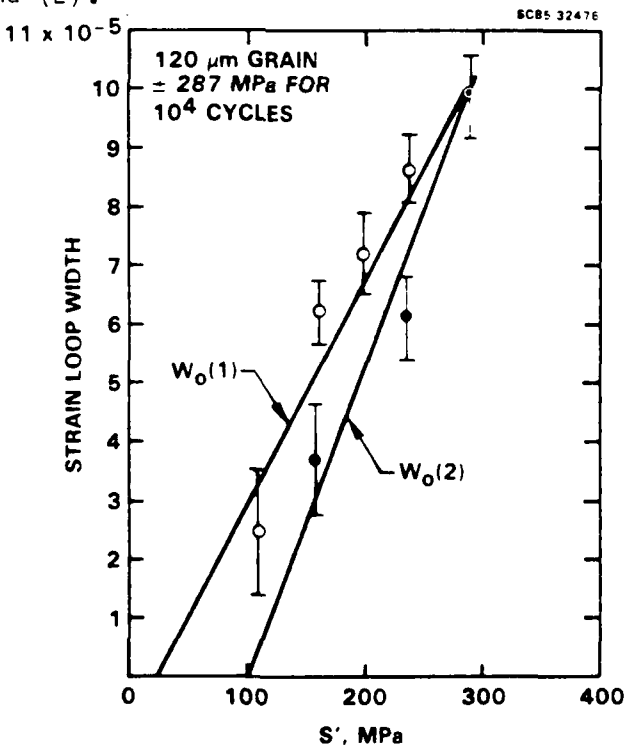

Fig. 4.5 Loop width vs s' for a 120 μm grain for load sequences (1) and (2).

Table 1

Deformation Properties

Grain Size	Apparent Deformation Depth	α	E^P MPa	σ_0 MPa	σ_y (0.2%) MPa
120 μm	< 2 μm	0.95 ±0.02	(9.0 ±3.5) × 10^4	100 ±20	280 ±60
330 μm	24 μm	0.78	0	225 ±10	225 ±10

The apparent depths of the deformation have been determined from Eshelby's equations by using measured major and minor grain axes at the surface and the calculated value of α. The values of the parameters obtained for the 330 μm grain are quite consistent with other results for σ_0 and E^P (described later) obtained by less elegant means. For grains in the 300 μm size range, fatigue apparently causes local softening to an approximately elastic-perfectly plastic state. Flow stresses as small as 140 MPa have been found, and there is less reliable evidence of even smaller values. The estimated 24 μm depth of deformation is consistent with the anticipated depth of the grain, but this agreement still must be tested by destructive analysis.

The result for the small 120 μm grain raises more questions than it answers, from a standpoint of the physics of localized deformation. Actually, for $p = q = -1/2$, there is no depth which will give $\alpha = 0.9$, but depths under 2 μm are consistent with this α within the range of experimental error. It appears that deformation in the 120 μm grain may be confined to a very shallow layer near its surface. A profiling of the true depth of this grain is also planned. But, other data suggests that such a shallow depth of the deformation is real.[13] Were the values encountered here for E^P and σ_0 common to all 120 μm grains, W_0 values of 2-4 × 10^{-4} would be anticipated for most grains of this size. Instead the 1 × 10^{-4} loop width reported here is an upper bound of the experimentally observed values.

The last entry in Table 1 deals with the apparent 0.2% strain offset yield strength of the grains. Remember with the stationary model σ_0 is identified as the stress below which deformation is elastic. σ_y (0.2%) was calculated for each grain by using E^P and σ_0 to construct a σ (local) vs ε_x (local) plot for the grain interior such as in Fig. 4.2. The 0.2% offset is then determined in the normal manner.

4.1.2 Analysis of Old Loop Width Data

Several years ago, James and Morris[13] measured W_0 at constant s for the same 2219 alloy studied here vs grain size, and at several intervals in fatigue. It is enlightening to look at these results with the stationary deformation model. To obtain an upper bound on the flow stress, we assume for this calculation $E^P = 0$ and an average value of $\alpha = 0.8$. Because σ_0 vs W_0 is double valued in the stationary model (see Fig. 4.1), there is an ambiguity in this analysis at large values of strain. In Fig. 4.6, we show results for fatigue at $\pm$ = 270 MPa after 10^4 cycles and present the maximum (4.6a) and minimum (4.6b) flow stress values found by the model. Included in both plots is a datum (x) giving the bulk flow stress, which is assigned a location at the average alloy grain size. For the solid circles, we have assumed that the flow stresses were progressively falling as the plastic strain increased. The open circles denote the ambiguous stress values; in a) we show the effect if σ_0 had started to rise, in b) if σ_0 continued to fall.

4.2 Flow Stresses Near the Grain Boundaries

From limited data, it appears that the flow stress within isolated microplastic grains may be reasonably uniform. Elastic deformation outside the grain is inferred from a comparison of measured strains vs distance from grain boundaries to the results of Eshelby (Sec. 4.2.1). Just inside microplastic grains a boundary region has been discovered which is distinguished by a reversal of the sign of W_0 at $\sigma^a = 0$ from that in the grain interior. The mechanics of the development of this boundary region are explained by an

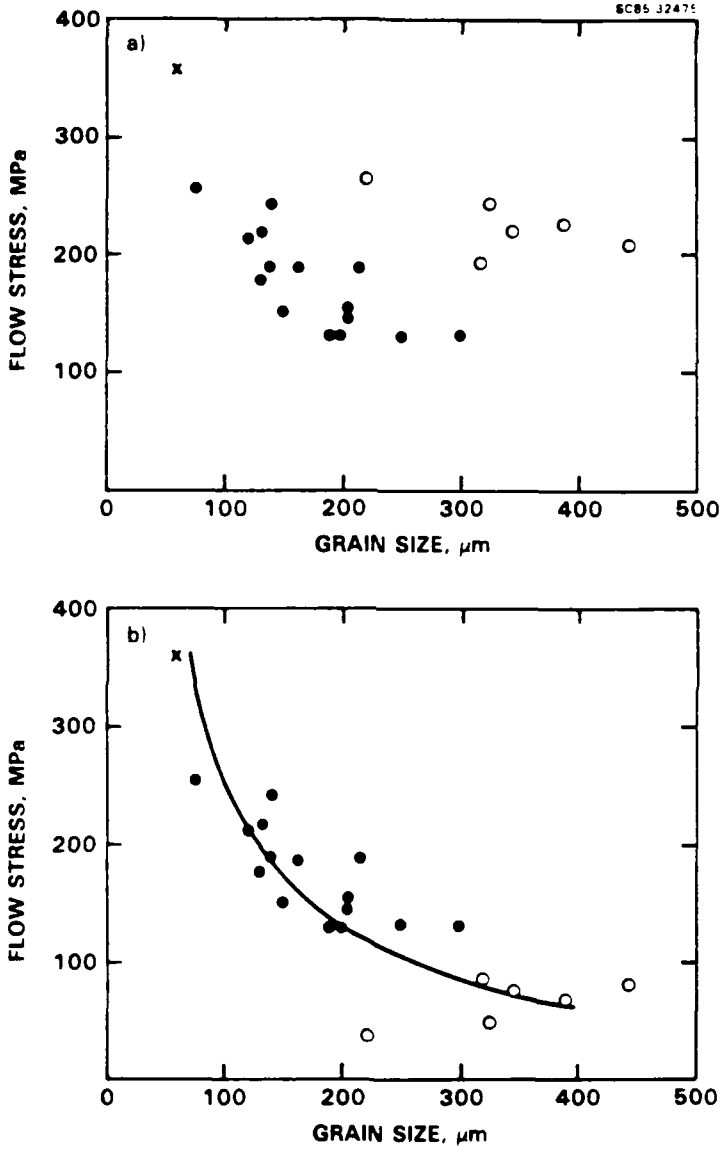

Fig. 4.6 Values of local flow stress for Al 2219-T851 fatigued 10^4 cycles at ± 270 MPa vs grain size. Calculated for an elastic perfectly plastic grain using the "stationary" deformation model. a) An upper bound to σ_0, b) the most probable σ_0 value. The curve in b) is a (1/grain size) function.

analysis provided by the dual domain deformation model. The reversal in sign of W_0 is a consequence of a flow stress in the domain close to the boundary being slightly higher than the grain interior (Sec. 4.2.2). Measurements show that outside the microplastic grain, the local flow stress rises abruptly to that consistent with the bulk value.

4.2.1 Elastic Matrix Response

Except for highly deformed sites discussed in Sec. 4.3, the deformation outside the isolated microplastic surface grains is indistinguishable from elastic. Reaction strains resulting from the confine plasticity have been compared to those calculated using Eshelby's equations for several grains, of which results in Fig. 4.7 are an example. Figure 4.7a is of ε_x along the transverse grain axis and 4.7b gives ε_y along the longitudinal grain axis (see Fig. 2.1). The solid curves in the elastic region just outside the grains have been calculated from the strains just inside the grain

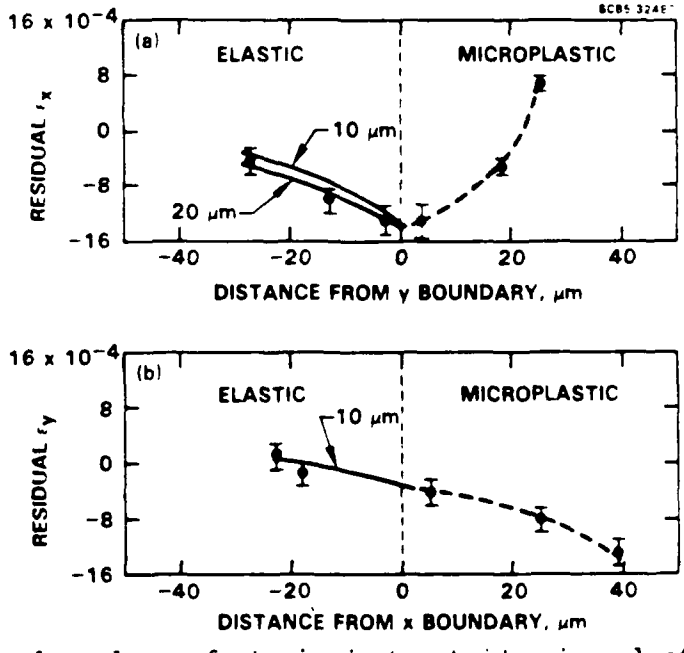

Fig. 4.7 Example values of strain just outside microplastic grains indicating an elastic matrix and deformation depths around 10 μm - the typical grain depth. NSF[1] data.

for several assumed depths of the plasticity and suggest that the microplastic deformation depth is comparable to the grain depth. We estimate that the sensitivity of our strain measurements precludes the distinction between values of σ_0 outside the grain which are larger than ≈ 300 MPa.

A completely unanticipated observation is that strains in the microplastic grain at the transverse boundary (Fig. 4.7a) are compressive after tensile loading. The results shown are after a half tensile loading cycle. Tensile strains would be anticipated from a uniform stationary deformation model. About 30 additional such measurements made under NSF funding confirm this result. In the grain interior, W_0 is positive, but a boundary layer some 20 μm in width is found in which W_0 is negative. An explanation of this behavior is found in analysis of stress-strain response vs applied stress using the dual domain model.

4.2.2 Flow Stress vs Location Within a Grain

By means that are explained momentarily, we have obained flow stresses (σ_0) shown in Fig. 4.8 along the y axis of a 270 μm grain after fatigue cycles. In setting the dashed line, we allowed ourselves to believe that the data are consistent with a σ_0 equal to the bulk flow stress just outside the microplastic grain. Also, since the value of $E^P = 1 \times 10^{+3}$ MPa is found inside the grain, $\sigma_0 \approx \sigma_y$ (0.2%). The boundary layer mentioned in Sec. 4.2.1 is only apparent in the strain loop width (W_0) (see Fig. 4.9). We have only a few points and have used our experience from strain measurements in other areas to place a dotted line through the values of W_0 measured at $\sigma^a = 0$ after a tensile loading cycle.

An explanation for the reversal in sign in W_0 at the boundary is found in the analysis of loop widths measured at sites in the grain vs σ^a. The experiment involved the measurement of strains over a partial tensile cycle, beginning and ending at the same value of σ^a (Fig. 4.10). The reversal in sign of W_0 at the boundary occurs automatically in the dual domain model if

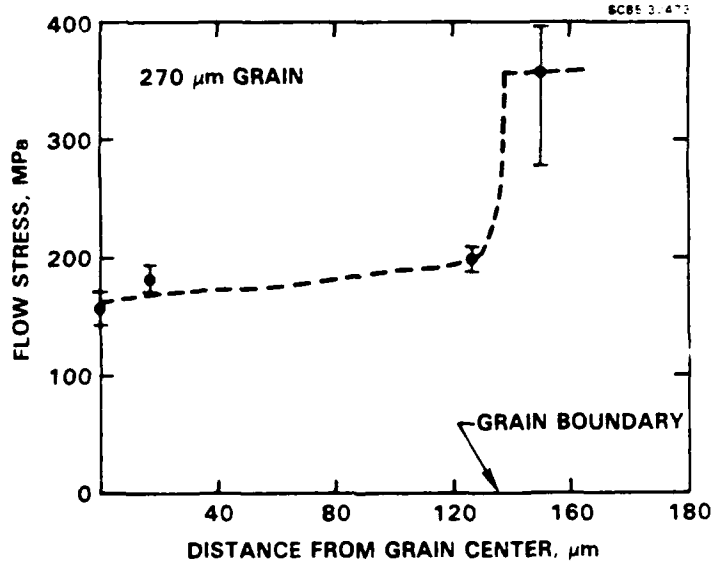

Fig. 4.8 Values of σ_0 extracted from local loop width data for a 270 μm grain using the "dual domain" model.

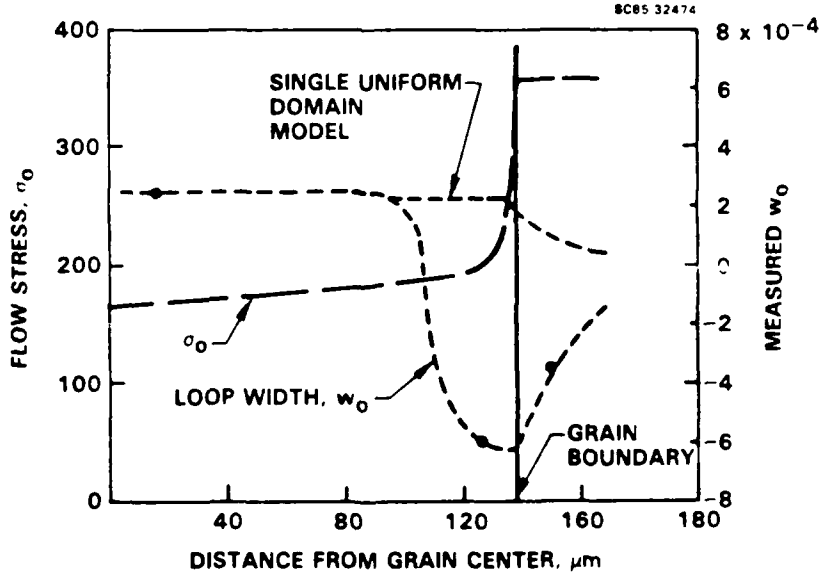

Fig. 4.9 Illustration of the location of the strain anomaly at a grain boundary and flow stress values associated with the anomaly.

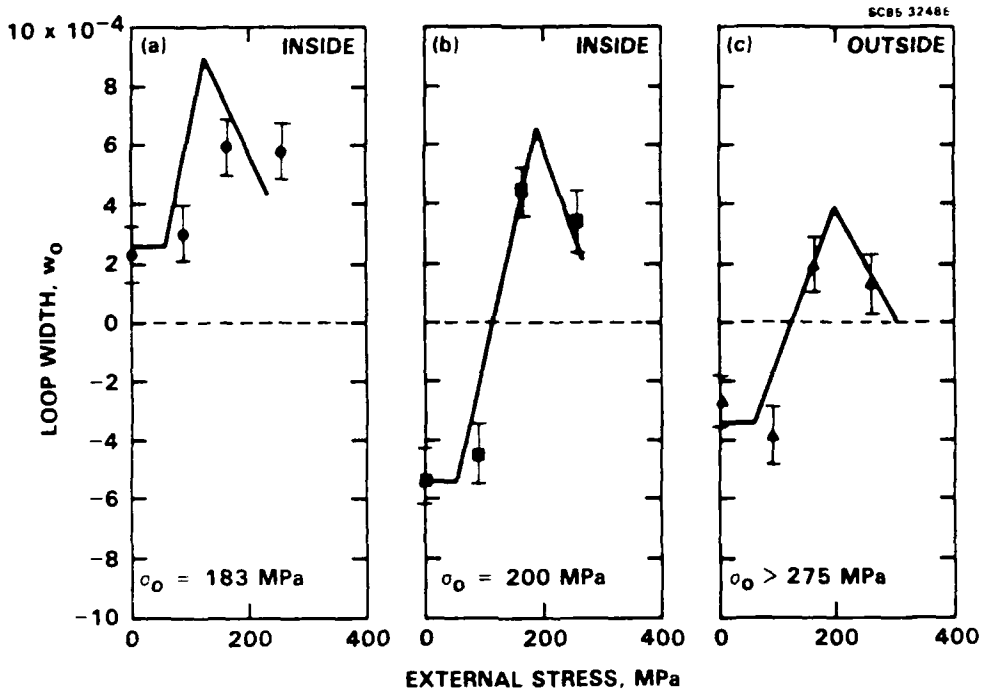

Fig. 4.10 Experimental values of loop width vs the external stress at the beginning and completion of the loading cycle. Data are for three different locations and curves are from the "dual domain" model, with $E^P = 1 \times 10^3$ MPa and the flow stress indicated. NSF[1] data.

σ_0 at the boundary is greater than in the interior of the grain, provided that E^P is within a very narrow range of values near 1×10^3 MPa, and also that α at the boundary is small. Under this condition, the stress (external) - strain (local) hysteresis loop can have the complex shape shown in Fig. 4.11. This is the loop shape which produces the result in Fig. 4.10b. At $\sigma^a = 0$, the motion about the loop is anticlockwise, but at large $|\sigma^a|$ the motion is conventional. An extensive search of the possible combinations of E^P, α and σ_0, which give quantitative agreement with the data of 4.10 has been used to establish error bars on the values of σ_0 given in Fig. 4.8. Anomalously small values of α are needed to describe the experimental results, however, and suggest that the boundary constraint is still not fully understood. We consider this aspect later (Sec. 5.0).

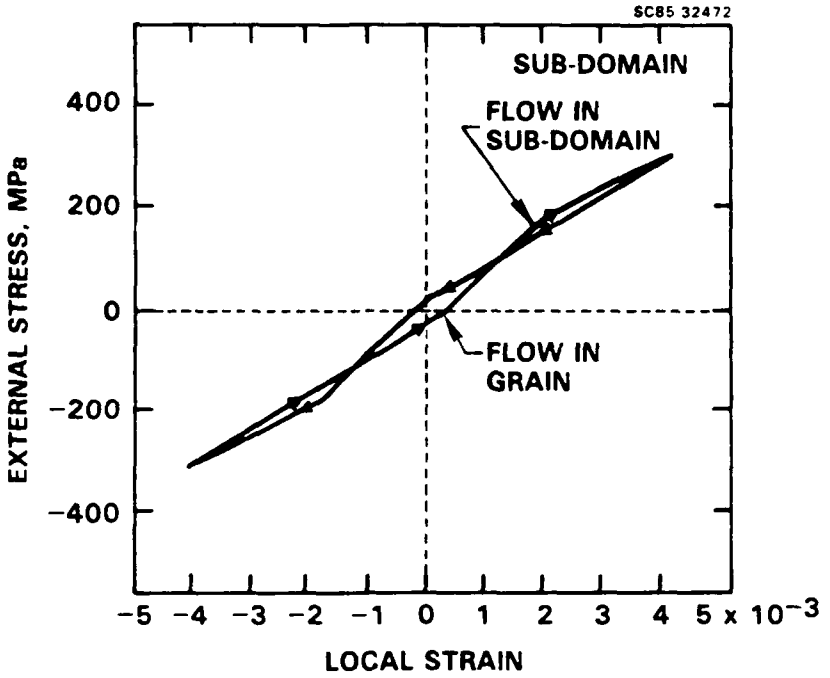

Fig. 4.11 External stress-local strain behavior at a boundary harder than a grain interior for appropriate α and E^p, predicted by the dual "domain model" has a characteristic structure useful for analysis of local flow stress values.

4.3 Flow Stress Evolution

We do not yet have a model for the variation of local flow stress with fatigue. σ_0 must be related both to grain size and to load spectra. However, an analysis (Fig. 4.12) of localized strain data obtained at constant amplitude does provide some insight into trends in σ_0 with grain size and fatigue cycles in the Al 2219-T851 alloy. The values given in Fig. 4.12 have been extracted from strain measurements previously obtained by James and Morris,[13] by using a homogeneous stationary deformation model. The analysis involves several assumptions which remain to be tested. In particular, for large grains the stress-strain loop widths are observed to increase to a maximum and then decrease with progressive fatigue. For the 350 μm grain case in Fig. 4.12, we have taken the flow stress consistent with observed loop width values, by assuming that σ_0 continues to fall after the maximum W_0 is reached. However, there are three other possibilities, namely

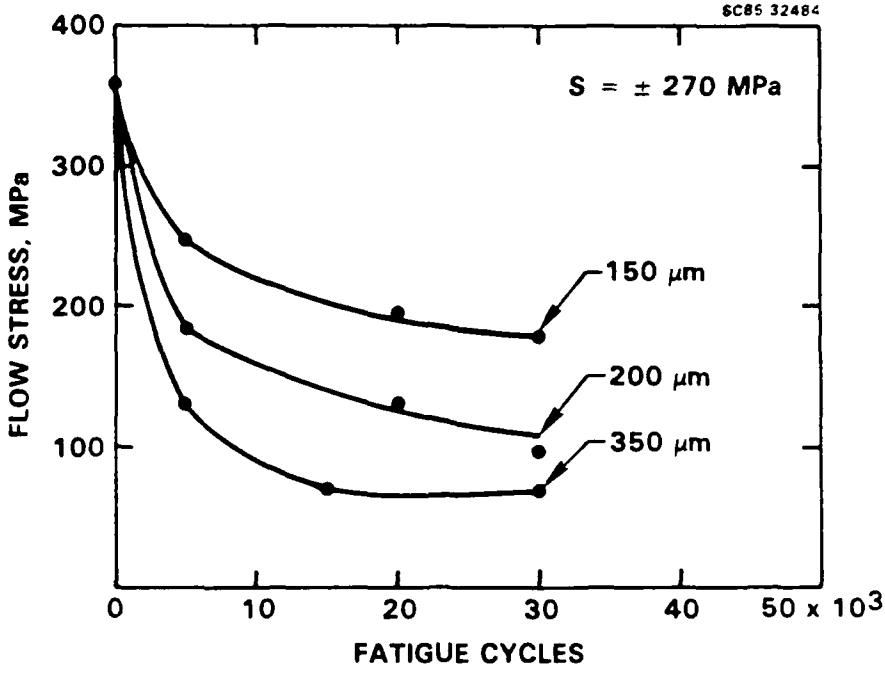

Fig. 4.12 Calculated values of local flow stress with fatigue obtained by averaging values for a number of grains of sizes near those indicated. Values less than about 140 MPa are less credible because they are very model sensitive.

a) σ_0 itself reaches a minimum and then increases;

b) E^p increases;

c) The grain boundaries soften, decreasing the applied stress range in the grain center.

We have looked at several special cases of very large grains (330 μm and larger) and it is clear for these that plastic deformation of the boundaries and the neighboring grains is partially responsible for the observed loop closings. The breakdown of the boundaries is accompanied by violent variations in localized strains which are associated with slip banding in the 2219 (Fig. 4.13) and, for very large grains (~ 500 μm), W_0 in the grain interior measured over a tensile loading cycle, actually becomes compressive (Fig. 4.14). This is behavior reminiscent of that in the hard boundary zones

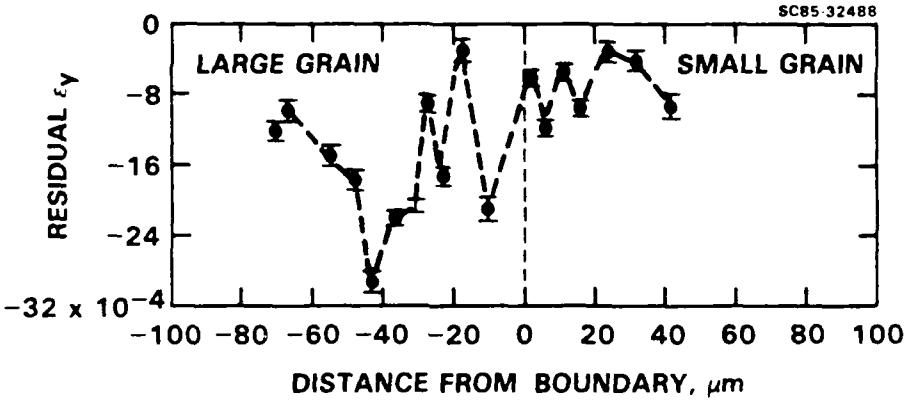

Fig. 4.13 Residual component of ε_y induced by tensile loading after fatigue has begun to disrupt a grain boundary. NSF[1] data.

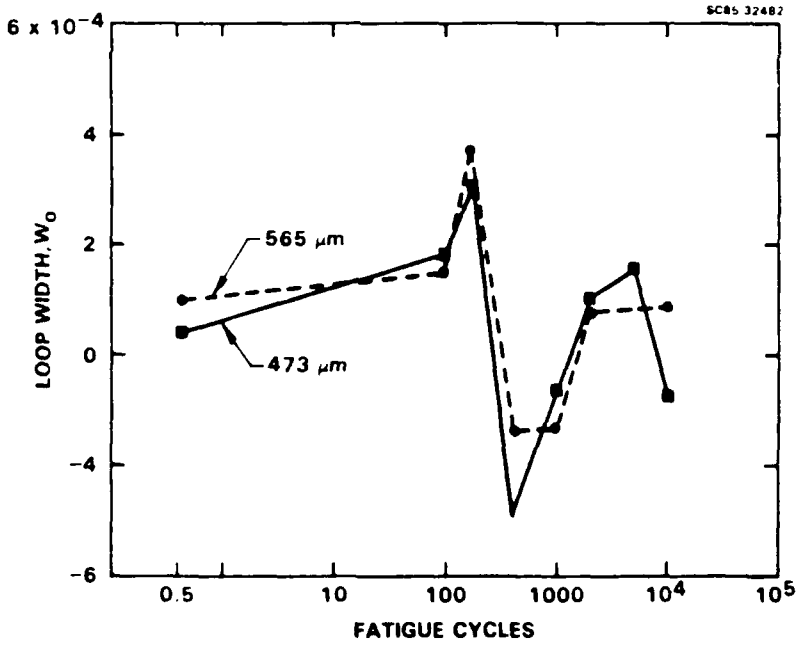

Fig. 4.14 Progress fatigue induced change in W_o for two large grains for s = ± 305 MPa. The compressive response after 500 cycles shows that the deformation is highly nonuniform, and that the grain interior is probably harder than the surrounding matrix.

described previously and suggests that a condition has been reached in which the grain interior has hardened relative to the surrounding medium.

4.4 Response to Spectrum Loads

The bulk of our information on the effect of spectrum loads has already been shown in Sec. 4.1. Initially, the only thought behind the data collection was to provide a basis for testing of the local deformation models vs load sequence. Later, we realized that with an appropriate analysis, the response to step changes in load could also be used to acquire estimates of the important parameters representing the deformation properties of the surface. At the same time, it is clear from the concurrence of the results with theory that major features of local stress-strain behavior are influenced in a predictable way by local reaction stresses created in response to the plasticity. A plastic grain acts in a fashion similar to a microscopic notch. Numerical calculations have been made of the deformation of plastic grains under positive and negative mean stresses and a ratcheting of the local deformation to achieve a local state of fully reversed loading is found, just as would occur at a notch. This response for surface deformation is consistent with x-ray diffraction observations of surface residual stresses in aluminums by James and Morris.[16] A next step in testing understanding of this behavior would be to collect strain response data within grains under nonzero mean loading. However, this research needs to be carefully integrated with an examination of the nature of the stress-strain and yielding behavior of the fatigue softened areas. As noted in Sec. 2.0, we have to this point relied heavily on a "stationary" yielding assumption and the analytic and experimental tools are now in hand to test this assumption and to compare its predictions to those from a "kinematic" yielding model. Remember that one difference between the two models is that there is no intrinsic Baushinger effect in the stationary model. The Baushinger response seen when the stationary model is invoked stems from the reaction stresses developed when the plastic deformation of a grain is confined by an elastic matrix. On the other hand, the

kinematic model material has its own internal memory of the stress history to which it has been exposed. Interestingly, however, the strain in a grain subject to a kinematic yielding assumption reaches a new equilibrium in just one complete cycle if a step change in the cyclic stress amplitude is made. Experimental observations (Fig. 4.15) indicate that several cycles are actually required for such an equilibrium to be achieved. However, before conclusions are drawn from this observation, the computer simulations of response under the locally biaxial stress state caused by plastic deformation should be examined carefully in the light of additional experimental observations.

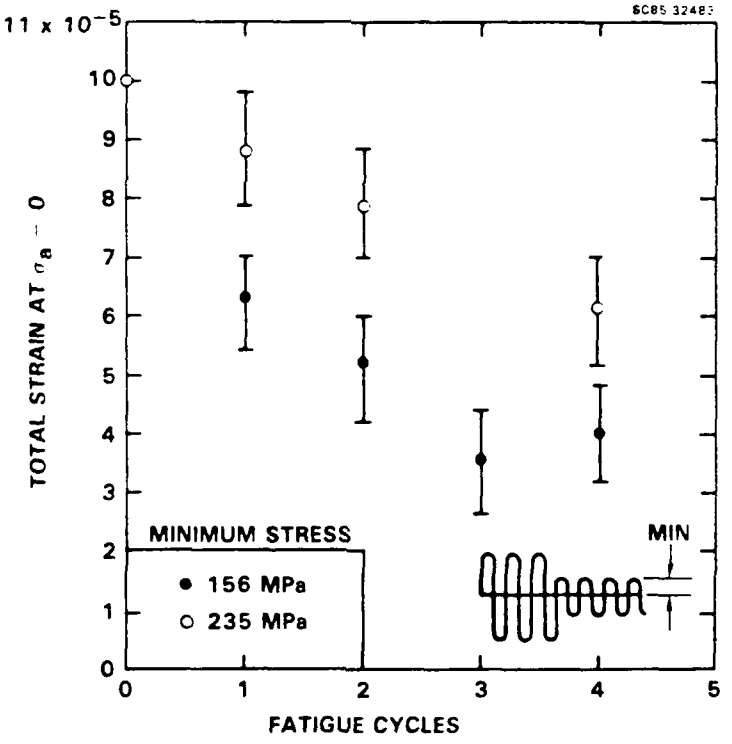

Fig. 4.15 Transient response in loop widths after a step change in cyclic stress amplitude. In this example, the initial stress range was ± 305 MPa and was then dropped to ± 156 MPa, in one experiment, and from ± 305 MPa to ± 235 MPa in a second experiment.

5.0 DISCUSSION

We believe that we have now identified the major building blocks which must be included in a model of crack initiation in fatigue under spectrum loads, at least for structural aluminum alloys. One key is that the softening of the surface which occurs with fatigue is extreme and localized to large grains. The values we obtain for local flow stresses are to a degree dependent upon the deformation model used to analyze the data, but there is no doubt that the stresses become very small. For Al 2219-T851 values of σ_0 below 140 MPa are credible, whereas the bulk cyclic yield strength is 360 MPa. Furthermore, the material in a softened grain responds in nearly an elastic-perfectly plastic fashion. Seeing this, it is little wonder that no endurance limit has been found for aluminum alloys. Only under very severe conditions such as for large cyclic stresses (perhaps 85% of the bulk elastic limit), and large grains (perhaps 350 μm), is there clear evidence that plasticity extends beyond a microplastic grain into neighboring grains. In addition, it is found that the local flow stresses change slowly with fatigue.

Over the years, we have had a chance to look in detail at the crack initiation behavior in aluminum alloys and especially in the Al 2219-T851 material used in this study. For constant amplitude fatigue, at lifes in excess of 10^5 cycles, crack initiation in the 2219 is entirely at constituent particles which lie within large grains on a specimen surface. Only at short lifetimes is grain boundary cracking apparent, and normally it is still the constituent particle cracking which produces the fatal crack. To us this suggests that the latter stage of deformation of the surface in which the boundaries of and neighbors to a large grain begin to deform does not necessarily have a consequence to lifetime. Its pertinence depends upon the availability of competing sites for initiation in the grain interiors which soften first. Only in compression dominated spectra have we found boundary cracking in 2219 to be of special importance.

With just these insights, we outline the structure of a model of crack initiation for spectrum loading and delineate the questions which must still be answered to complete and test the model (5.1). Following that, we examine what we have learned that bears upon answers to these questions for Al 2219-T851 (5.2).

5.1 Future Initiation Modelling

Initiation modelling requires a physically correct representation of localized microplastic deformation. Some approximations are unavoidable and should be used if they are supported by experimental evidence. We suggest the following model of crack initiation inside an isolated microplastic grain is appropriate.

Grain Properties and Deformation Model

Grain embedded in an elastic matrix
Ellipsoidal grain
Uniform deformation - response controlled by internal reaction stress

Material Properties with the Microplastic Grain

Approximately elastic-perfectly plastic
Cycle dependent flow stress

Need
- [Yield Model]
- [σ_0 cycle and grain size dependence]
- [More deformation depth information]

Initiation Criterion - Possibilities

Need Criterion
- Peak plastic strain range
- Integrated plastic strain
- Integrated hysteretic energy

If the fatigue induced softening of a grain continues progressively, then the peak and integrated plastic strains will follow suit. But, the hysteretic energy per cycle will decrease with sufficient softening (as shown in Sec. 2.4). Our particular interest in this latter observation is that in 2219 crack initiation in large grains tends to occur in a sudden burst of activity, if a specimen is fatigued at constant amplitude. If cracking ceases because E^P or σ_0 begins to increase at some point during fatigue, then the same change in initiation behavior will be seen at all amplitudes. But, if softening and hysteretic energy are involved, this cessation of initiation will pertain only to constant amplitude. The loop width equations for the "stationary" deformation model show that, instead, a low-high amplitude block loading sequence will be much less damaging than a high-low sequence. This is a trend which is supported by experiment for 2219.[15] So an important step in the model development is to determine the driving force for initiation. This can easily be done once progressive changes in σ_0, E^P and W_0 have been determined within selected grains during fatigue, using the technique described in Sec. 4.1.

The theory then requires a model to calculate from cycle-by-cycle local strain values the fatigue induced change in σ_0, and a correct representation of the local strains encountered in any arbitrary loading sequence. The latter is essentially provided by the procedures described in Sec. 2.3. What is still missing is knowledge of the yield criterion. For a material which is nearly an elastic-perfectly plastic material, such as we find for softened 2219 grains, the "stationary" and "kinematic" deformation models should demark the two extremes of the expected deformation behavior. In fact, if $E^P = 0$, the two yield criteria are identical. At this juncture, one needs

to look more carefully at the biaxial strain predictions of these models to identify critical experiments which would be useful for model validation.

5.2 Local Mechanical Properties

The solution we seek for prediction of fatigue initiation lifetime has been reduced to that of a problem in micromechanics. Models and their numerical implementations to calculate local stress-strain behavior in a microplastic grain have been developed, and for fully reversed loading, a "stationary" local yielding criterion provides an acceptable representation of experimental observation. Fulfillment of our initial goal requires a better understanding of the way in which the material mechanical properties (such as flow stress) and the local yielding criterion evolve with fatigue. A calculation of the local stress-strain response in an ellipsoidal grain for arbitrary loads awaits only this final insight. Although we know that the deformation within a grain can be complex, especially near boundaries, it appears that an assumption of uniform deformation within the grain interior will suffice for our modeling objectives so long as the important crack initiation is actually at such interior sites.

As described by Margolin[17] and Asaro[18] several years ago, any local inhomogeneity in deformation automatically provides the foundation for Bauschinger and load history effects. These arise because of reaction stresses generated by constraint of the nonuniform deformation. For microplastic grains in 2219 we find that these constraining stresses are huge because the local values of flow stress become very small during fatigue. Herein is the major problem in analysis of surface microplasticity. The local and applied stresses differ substantially and only the strains and applied stress are experimentally available. Appropriate theories, experimentally validated, are needed to discern the local mechanical properties and yielding behavior almost hidden from view by the reaction stresses.

This is what we now know about the mechanical properties of microplastic grains in 2219. The most reliable values for properties in a small

(120 μm) grain are reported in Table 1. Although the data were obtained after fatigue, we think it is likely that the numbers represent the ambient prefatigue values of the surface. It was necessary to measure surface strains in the 10^{-5} range to obtain the parameter values of σ_0 = 100 MPa and E^P = 1.3×10^4 MPa for this example. Bulk materials are known to have a two-step yielding behavior and the 100 MPa value would correspond to the lower yield point for the grain. It happens that the apparent depth of the layer with this flow stress is only 2 μm; this is typical of the dislocation cell size in Al - suggesting a possible connection. This would mean that E^P for the cell structure would be in excess of 10^4 MPa. Values of σ_0 for 100 μm grains given in Fig. 4.6 are quite consistent with this result. Remember, the estimates shown in Fig. 4.6 are actually upper bound estimates of σ_0 in that we have assumed that $E^P = 0$, independent of grain size in calculating the σ_0's given. Supporting evidence that the mechanical properties found for the 120 μm grain may be universal in 2219 is apparent in Fig. 4.4. In these loop width results for a 330 μm grain, a small positive plastic strain is found below the $s' = \sigma_2$ axis intersection point, contrary to the "stationary" deformation model $W_0(2) = 0$ prediction. It happens that the very small residual strain present is just those that would be anticipated if there were an earlier yield point in the grain with a plastic modulus of about $E^P \sim 10^4$ MPa for a stress below σ_2.

The fatigue-induced softening of the surface of 2219 appears to involve the development of long-range slip extending grain wide. The bands are not seen by optical microscopy, but are apparent in strain field measurements made over the entire surface of a grain [NSF[1] result]. We think it is this longer range dislocation structure which exhibits an elastic-perfectly plastic (i.e., $E^P = 0$) deformation behavior. A recent paper by Laird, to be published shortly, shows that the fatigue of dispersion-hardened single copper crystals produce banding and a drop in flow stress to a value approaching that of the unalloyed copper. This happens for a plastic strain in the range of $1\text{-}5 \times 10^{-3}$, numbers typical of those seen for Al in this study. Only at higher plastic strains is hardening and the development of a tangled disloca-

tion structure apparent. If the same phenomenon were active in the single-grain crystals of 2219 at the surface, it would produce essentially the same characteristic changes in local flow stress with fatigue that we have reported here. Only the dynamics of the softening must be more complex, because in a surface grain the local plastic strain range changes cycle-by-cycle. Nevertheless, the net effect on the local σ_0 should be the same.

The mechanical properties near grain boundaries in 2219 are more nebulus. Clearly, early in fatigue the boundaries are harder than the grain centers. But, despite the obvious success of the dual domain model in simulating boundary stress-strain response, there is an inconsistency in the model. The problem concerns $\alpha(2)$, the relative reaction stress parameter at the boundary. To explain our observations, approximate values for $\alpha(2)$ of 0.7 are required. While boundary zone structures can readily exist which produce such an $\alpha(2)$, there is no obvious zone shape which would create such a layer along the entire length of the boundary. Yet, that is exactly what is observed.[1] It appears that application of the free surface correction to our model does lower the boundary α values somewhat, but probably not enough to explain what we see. An additional consideration is that the triple points in the boundary are also soft spots.[1] The fact is that deformation near the boundaries is complex and is still poorly understood.

A second key to understanding the behavior of deformation localized in a single grain is that the measurable hysteresis loop widths in the grain are very small because of the constraint provided by the surrounding elastic matrix. Despite this, the local plastic strains can be large. They must approach 1×10^{-2} in some grains we have examined. This means that the elastic reaction stresses in a grain are also very large. Herein, apparently, is the source of many load amplitude and sequence effects. The mean stress and stress range experienced in the elastic-plastic material within a grain is derived from both the external stress and from a reaction stress which depends upon the immediate state of plastic strain in the grain.

Much of what was previously known about the properties of grain interiors vs boundaries in metals comes from a few monotonic deformation studies. Except at triple points, the boundaries are typically found to be harder than the grain centers. But, these are bulk deformation observations and the applied plastic strains are larger. Even the differences in flow stress found between boundaries and the grain interior have been relatively small. So our findings regarding the fatigue-induced softening of Al 2219-T851 are a major revelation of the physics and mechanics of surface deformation. The results are essential to an understanding of crack initiation. They also have immediate application to the understanding of fatigue-induced changes in residual surface stresses. Additionally, they provide a probable explanation for the persistence of propagation of short cracks in a surface even at cyclic stress intensities well below the long crack stress intensity range threshold. Now we realize that the surface is not even approximately elastic. The small surface cracks initiate in large grains and are embedded in a highly microplastic surface layer. These insights have come in quite a rush as this program has drawn to completion and papers detailing our results are still in preparation. The first, entitled, "Microplastic Surface Deformation of Al 2219-T851," will be submitted to Acta. Met.

6.0 SUMMARY AND CONCLUSIONS

Fatigue cracks in structural aluminum alloys commonly initiate at the surface. Lifetimes depend on the alloy microstructure, especially on grain size, and show a distribution apparently controlled by stochastic cracking processes which are associated with individual grains at the surface. Conventional cumulative damage methods are applicable to aluminums, but there are cases where they do not work well. Also, they are especially inept in predicting stochastic behavior for spectrum loading, and are useless in a priori predictions of the consequences of variability in the material properties. With the goal of defining a methodology for making initiation lifetime predictions on the basis of physical insight into the micromechanics of the local deformation processes, this research has focused on the properties of the localized regions in the surface at which cracks initiate. This has involved rather sophisticated measurements of localized strains in the surface in individual grains, and frequently, over very short gauge lengths. But, the main thrust of the program has been the development of the theoretical tools to analyze our experimental data. The major challenge is that the localized plastic strains are large, and reaction stresses created by constraint of the plasticity are also large. As a consequence, the local stresses differ substantially from the applied, making it impossible to directly measure local yield strengths and plastic moduli within grains under study. The theoretical models of deformation are needed to extract from measurements in a grain of total-strain vs external load, the true plastic strains and the material mechanical properties which vary from grain to grain. The models also need to establish from the data the mechanisms by which these local mechanical properties change with fatigue and also the criterion which controls local yielding within a grain. These analysis goals can only be accomplished by a model which, although it may be an approximation, embodies the essential physics and mechanics of the deformation process. The advantage of this approach is that once the mechanical property and yielding behavior is understood, the deformation model then becomes the crack initiation model. The theory is used to

calculate the local stress-strain response within a grain subject to microplasticity and under conditions of arbitrary load spectra. All that is required to complete the initiation lifetime prediction is knowledge of the crack initiation criterion. Criteria such as critical values of accumulated total plastic strain, or cumulative local hysteresis energy per cycle are postulated and validated by experiment. Modelling of the stochastic behavior can then be approached by numerical techniques which sample the lifetime response conditioned on a distribution of grain sizes and critical initiation parameter values. By this point, however, the treatment of the difficult spectrum loading aspects of the problem is already directly embedded in the model of localized deformation and requires no further attention.

We have made substantial progress in the development of such a formalism. The first generation of deformation models are complete and they have lead to startling discoveries about the mechanical properties of the surface of the structural Al 2219-T851 alloy which has been the model material used in our study. We have also gained substantial insight into the conditions under which the approximations in the deformation models will be valid, and information on the way the localized mechanical properties within grains change with fatigue. Needed to complete the initiation methodology is a physical model of these property changes in relation to local grain size and to the local stress-strain environment. Also more must be learned about the local yield criterion, and experiments are needed to establish which is the most appropriate local crack initiation criterion. Thereafter, remaining work on the predictive methodology will simply be numerical modelling to collate these insights and validation studies of the lifetime predictions.

In summary, the following has been accomplished.

6.1 Theoretical Modeling

1. A numerical implementation of Eshelby's equations to calculate the elastic strain and stress fields surrounding a plastically deformed grain has been completed. Results for selected grain shape showed that the fields external to the grains might be sufficiently large to damage regions near the boundaries, but probably were too small to produce stress-strain behavior conditioned on neighboring grain interactions. This led to the focus of subsequent work on the deformation inside individual microplastic grains and at their boundaries. Later, careful comparisons of predicted and measured strain fields outside of microplastic grains showed that a common condition was for the matrix surrounding microplastic grains to be elastic. The external elastic strain magnitudes were also used to calculate the depth of the microplastic strains within individual grains. The deeper the plasticity, the more slowly the elastic fields fall off with distance from the grain boundary. These comparisons gave values for plasticity deformation depths which were typical of the average grain depth, suggesting that the microplastic deformation extended to and was also interrupted by the subsurface boundaries.

2. A numerical procedure was developed to calculate from Eshelby's solutions the correct stress and strain fields inside and outside of a microplastic grain in the presence of a free surface. Results of sample calculations show that if the plastic deformation within a grain is uniform and volume conserving, the effect of the "free surface" correction is too small to be seen with our current experimental sensitivity. However, a singularity in the deformation is found at the boundary at the surface. This must be relaxed by plastic flow. This condition may modify the boundary constraint and make itself visible through the indirect effect of the changed constraint. For example, we have assumed that there is no sliding at the boundary between the microplastic grain and the external elastic matrix. If the singularity promotes sliding, strains near the boundary would not be correctly given by the Eshelby model.

3. An unanticipated result of strain measurements near the boundaries of microplastic grains was the discovery of sites in which motion about an external stress-local strain hysteresis loop was anticlockwise. Under NSF[1] funding, an explanation for this phenomenon was sought in the consideration of a dual-domain model in which a second region of uniform deformation was embedded at the boundary. The boundary domain was allowed to have mechanical properties different than the remainder of the grain. Analytic expressions for some of the simpler stress-strain behaviors of this composite structure were derived. These showed that with appropriate parameters a dual domain structure could produce the observed anticlockwise motion at the boundary, while deformation in the center of the grain retained the normal clockwise motion. The boundary behavior is the result of stress fields generated by constraint of the boundary domain by the rest of the microplastic grain. Under NAVAIR/NADC funding a numerical procedure was developed to calculate the stress-strain response for arbitrary material parameters and local yield strengths. By comparing results of calculated stress-strain behavior of this model with experimental data, flow stresses were determined for Al 2219-T851 as a function of location within a large microplastic grain. These values were much smaller than the bulk yield strength and nearly uniform within the grain. Near the boundaries and inside the grain, an abrupt increase in flow stress was found, and just outside the grain, the strains were indistinguishable from that resulting from elastic deformation.

4. The early "dual-domain" model was derived using a von Mises criterion for a uniaxial stress state or "stationary" plastic deformation criterion. The calculation was also uniaxial - the transverse fields created by constraint of the microplastic grain being neglected. This model lacks a Bauschinger effect internal to the material. In fully reversed loading, the Bauschinger response predicted stems from a reaction stress caused by constraint of the microplastic grain. However, with arbitrary load

sequences, the absence of an internal stress state in the material itself becomes quite apparent. To increase modeling flexibility, a numerical procedure was developed to calculate stress-strain response which included the biaxial field and for a Prager or "kinematic" yielding criterion. Also, simple analytic expressions for some of the deformation behaviors of the models were derived and examined. These included descriptions for the stress-strain hysteresis loop widths for constant amplitude and for step changes in external stress range. It was found that transient variations in loop width with a stress range change were intrinsic to the "stationary" model, but absent beyond the second cycle after stress range change with the "kinematic" model. For the "stationary" model a procedure was devised to calculate, from experimental data, local values of flow of stress (σ_0), plastic modulus (E^P), and the depth of the microplastic deformation within a grain. Application involved the obtaining of loop widths for a prescribed series of loading sequences, including determining the consequence of change in stress range as a function of the new stress amplitude. In concurrence with the dual domain results, values found by this technique for a large (330 μm) grain after 500 fatigue cycles were σ_0 ~ 225 MPa and E^P = 0 MPa. This should be compared to a bulk cycle yield strength for Al 2219-T851 of 360 MPa.

5. Options to replace the dual domain model of deformation of a microplastic grain have been explored. Numerical implementation of a procedure to calculate a physically accurate three-dimensional distribution of strains and stresses within a grain is practical. This would give a much better insight into the mechanism of evolution of the deformation, especially at the grain boundaries. However, an analysis showed us that code could not be developed within the scope of this program and this activity was terminated.

6. As a precursor to a selection of the correct criterion for crack initiation within a grain, the behavior of the hysteretic energy criterion was

examined in terms of its response to material parameters such as local flow stress and plastic modulus. We find, for example, that in the "stationary" deformation model the energy deposited into the grain per cycle goes down if the flow stress drops below a critical value. If accumulated hysteretic energy is driving the initiation, then the response of crack initiation rates to certain load sequences will have characteristic behaviors which should make identification of the energy criterion as the correct criterion relatively straightforward.

6.2 Conclusions About Deformation Behavior of Al 2219-T851

1. With the exception of very large (> 350 μm) grains at high stress amplitudes (> 85% yield), microplastic deformation is highly localized and contained within individual surface grains. This is confirmed by an equality between the elastic strain field predictions of Eshelby's model for sites external to a deformed grain and experimental observation.

2. Deformation strains within a grain can be treated as uniform except near the boundaries where anomalous stress-strain response has been found. The boundary constraint condition which leads to an anticlockwise motion about the external stress-local strain loop in a grain near the boundary is not completely understood. However, we have shown that a sufficient condition for the behavior is a slightly higher flow stress near the boundaries compared to the grain interior. A full understanding of this behavior is needed only for those materials in which crack initiation at the grain boundaries is an important process. However, this phenomena may influence the propagation of small cracks across grain boundaries.

3. Values of flow stress, plastic modulus and depth of deformation have been calculated for selected grains. More needs to be done to define the evolution of these properties, but presently, the following scenario appears likely. In the early stages of fatigue, only a very thin (~ 2 μm) layer

of the surface is microplastic. This depth is comparable to dislocation-cell sizes in aluminum, suggestive of a connection. The surface flow stresses is low (< 150 MPa compared to a 360 MPa bulk value), but the plastic modulus is very large (> 10^4 MPa). The plastic deformation experienced by the surface is therefore extremely small and indistinguishable from elastic except by the most sensitive of measurements. With fatigue, long-range slip develops in the larger grains in the surface. Experimental values of plastic modulus for these softened grains are $E^P \sim 0$. Thus, the material in the grains is essentially elastic-perfectly plastic. Accurate values of the flow stresses (σ_0) for some grains have been obtained by analysis of experimental measurements of loop widths for selected load sequences and load levels. These give σ_0 values of approximately 200 MPa after some hundreds to thousands of cycles of fatigue at stress amplitudes well below the bulk elastic limit. Less accurate estimates of flow stress based upon a single loop width measurement have been derived vs grain size, under the assumption that $E^P = 0$ for all grains. This analysis shows a flow stress decreasing with grain size, and uncovers examples of grains in which the apparent σ_0 after fatigue is less than 100 MPa.

6.3 Conclusions About Initiation Lifetime Modelling

1. Microplastic deformation which leads to fatigue crack initiation can be highly localized, being confined to individual large surface grains.

2. Because of the constraint of such localized plasticity by an otherwise elastic surface, stresses within a grain can depart markedly from that externally applied.

3. For an Al 2219-T851 alloy, a progressive fatigue-induced softening of a microplastic grain occurs. Local flow stresses apparently can fall to less than 30% of bulk cyclic yield strength values. The plastic moduli of

such grains are small and the deformation is nearly elastic - perfectly plastic.

4. The strains within a grain which control initiation can be calculated, at least within the grain interiors, with reasonable reliability. These respond to the external load spectra in a fashion determined by the deformation-induced reaction stress, in turn, established by the local flow stress. Herein is an obvious source of load amplitude and sequence effects on fatigue lifetime.

5. A complete procedure to calculate lifetimes on the basis of such a deformation model awaits the development of a model to relate progressive changes in flow stresses within a grain to the stress-strain history it experiences. Candidate criteria to describe the local onset of yielding should still be critically reviewed to refine the accuracy of predicted stress-strain behaviors during load transients. Finally, the identification of the controlling criterion for crack initiation must be made from several competing candidates. This criterion would be used to identify the time of initiation from predicted local strains in response to an applied spectra.

6. A capability to predict the stochastic initiation behavior of such a deformation model would entail development of numerical methods to collate the response of multiple potential crack initiation sites.

7.0 REFERENCES

1. "Fundamental Characterization of Surface Microscopy," NSF DMR-8310652, Aug 1983 - Jan 1986.

2. R. von Mises, Gottinger Nachrichten, Math.-Phys. Klasse, 582 (1913).

3. W. Prager, "The Theory of Plasticity - A Survey of Recent Achievements," Proc. Inst. Mech. Engrs., London 169, 41 (1955).

4. J.D. Eshelby, "The Determination of the Elastic Field of an Ellipsoidal Inclusion, and Related Problems," Proc. Roy. Soc. (London) A241, 376-96 (1957).

5. B. de Saint Venant, Comptes Rendus Acad. Sc. Paris 70, 473 (1870).

6. M. Levy, Comptes Rendus Acad. Sci. Paris 70, 1323 (1870).

7. J.D. Eshelby, "The Elastic Field Outside an Ellipsoidal Inclusion," Proc. Roy. Soc. A252, 561-9 (1959).

8. L. Prandl, Proc. 1st Int. Cong. App. Mech., Delft, 43 (1924).

9. A. Reuss, Zeits. ang. Math. Mech. 10, 266 (1930).

10. R.D. Mindlin, "Force at a Point in the Interior of a Semi-Infinite Solid," Physics 7, 85 (1936).

11. K. Tanaka and T. Mura, "A Dislocation Model for Fatigue Crack Initiation," J. Appl. Mech. 103, 97-103 (1981).

12. N.I. Muskhelishvili, "Singular Integral Equations," (Noordhoff: Groningen, Holland), 251 (1946).

13. M.R. James and W.L. Morris, "The Role of Microplastic Deformation in Fatigue crack Initiation," Fatigue Mechanisms: Advances in Quantitative Measurement of Physical Damage, ASTM STP-811, Am. Soc. Testing and Materials, Philadelphia, PA, 46-70 (1983).

14. W.L. Morris, "Microcrack Closure Phenomena for Al 2219-T851," Met. Trans. 10A, 5-11 (1979).

15. W. L. Morris, R.V. Inman, and M.R. James, "Measurement of Fatigue Induced Plasticity," J. Matls. Sci., 17, 1413-1419 (1982).

16. M.R. James and W.L. Morris, "Fatigue Induced Changes in Residual Surface Stress," Scripta Met., 17, 1101-1104 (1983).

17. H. Margolin, F. Hazaveh and H. Yaguchi, "The Grain Boundary Contribution to the Bauschinger Effect," Scripta. Met., 12, 1141-1145 (1978).

18. R.J. Asaro, "Elastic-Plastic Memory and Kinematic-Type Hardening," Acta. Met., 23, 1255-1265 (1975).

DISTRIBUTION LIST

GOVERNMENT ACTIVITIES

	NO. OF COPIES
AFWAL, WPAFB, OH 45433	
(Attn: FIBEC, Dr. G. Sendeckyj).	1
(Attn: FIB/L. Kelly, W. Goesch, C. Ramsey).	3
(Attn: FIBCA).	1
(Attn: FIBE/Mr. D. Smith).	1
(Attn: MLBM/Dr. J. Whitney, M. Knight).	2
(Attn: MLB/F. Cherry).	1
(Attn: MBC/Reinhart).	1
(Attn: AFWAL/MLSE/S. Fecheck).	1
DEPARTMENT OF THE AIR FORCE, Bldg. 410, Bolling Air Force Base, Washington, D.C. 20332	
(Attn: Dr. M. Salkind, Dr. Amos).	2
DEFENSE TECHNICAL INFORMATION CENTER (DTIC), Bldg.#5, Cameron Station Alexandria, VA 22314	
(Attn: Administrator).	2
FAA, Washington, D.C. 20591	
(Attn: J. R. Soderquist, AW-103).	1
FAA, Technical Center, Atlantic City, NJ 08405	
(Attn: L. Neri, Code ACT-330; M. Caiafa, Code ACT-033).	2
NASA HEADQUARTERS, Washington, D. C. 20546	
(Attn: Airframes Branch, FS-120).	1
(Attn: OAST/RM, Dr. D. Mulville).	1
NASA, George C. Marshall Space Flight Center, Huntsville, AL 35812	
(Attn: E. E. Engler, S&E-ASTN-ES).	1
(Attn: R. Schwinghamer, S&E-ASTN-M).	1
NASA, Langley Research Center, Hampton, VA 23365	
(Attn: Dr. J. R. Davidson, MS 188E; Dr. J. Starnes, MS-190; Dr. M. Mikulus, H. Bohan, and Dr. C. P. Blakenship MS 189M).	5
NASA, Lewis Research Center, Cleveland, OH 44135	
(Attn: Dr. C. Chamis, MS 49-6; M. Hershberg, MS 49-6).	2
NAVAIRSYSCOM, Washington, D.C. 20361	
(Attn: AIR-00D4).	1
(Attn: AIR-530).	1
(Attn: AIR-5302D).	1
(Attn: AIR-5302).	1
(Attn: AIR-5302F).	1
(Attn: AIR-53032D).	1
(Attn: AIR-931B).	1
NAVPGSCHL, Monterey, CA 95940	
(Attn: Prof. R. Ball, Prof. M. H. Bank, Prof. K. Challenger).	3
NAVSEASYSCOM, Washington, D.C. 20360	
(Attn: C. Zannis, SEA-05R25)).	1
NAVSEC, Arlington, VA 20360	
(Attn: NSEC-6101E).	1

DISTRIBUTION LIST

GOVERNMENT ACTIVITIES - (continued)

	NO. OF COPIES
NAVSHIPRANDCEN, Annapolis, MD 21403	
(Attn: H. Edlestein, Code 2870).	1
NRL, Washington, D.C. 20375	
(Attn: Dr. I. Wolock, Code 6122; Dr. C. I. Chang, and Dr. R. Badaliance).	3
NSWC, WHITE OAK LABORATORY, Silver Spring, MD 20910	
(Attn: Dr. J. Goff, Materials Evaluation Branch, Code R-34	1
(Attn: Dr. J. M. Augl).	2
ONR, 800 N. Quincy St., Arlington, VA 22217	
(Attn: A. Kushner Code 432/A; Y. Rajapakse, Code 1132SM)	2
ONT, 800 N. Quincy Street, Arlington, VA 22217	
(Attn: Cdr. D. Brown, (OCNR-212).	1
PLASTEC, Picatinny Arsenal, Dover, NJ 07801	
(Attn: H. Pebly).	1
(Attn: Librarian, Code DRDAR-SCM-O, Bldg. 351-N).	1
ARMY MATERIALS TECHNOLOGY LABORATORY Watertown, MA 02171	
(Attn: D. Oplinger, SLCMT-MS).	1
U. S. ARMY APPLIED TECHNOLOGY LABORATORY, USARTL, (AVRADCOM), Ft. Eustis, VA 23604	
(Attn: J. Waller; T. Mazza).	2
U. S. ARMY AIR MOBILITY R&D LABORATORY, Ft. Eustis, VA 23604	
(Attn: H. Reddick).	1
U. S. ARMY R&T LABORATORY (AVRADCOM), Ames Research Center, Moffet Field, CA 94035	
(Attn: F. Immen, DAVDL-AS-MS 207-5).	1
U. S. NAVAL ACADEMY, Annapolis, MD 21402	
(Attn: Dr. R. D. Jamison, Mechanical Engineering Department).	1
DAVID TAYLOR NAVAL SHIP RESEARCH & DEVELOPMENT CENTER, Annapolis, MD 21402	
(Attn: E. T. Camponeschi, Code 2844; R. Crane, Code 2844).	2
DAVID TAYLOR NAVAL SHIP R&D CENTER Bethesda, MD 20084	
(Attn: A. Macander, Code 1720).	1
NAVAIRDEVCEN, Warminster, PA 18974	
(Attn: Code 8131).	3
(Attn: Code 09L2).	2

DISTRIBUTION LIST

NON-GOVERNMENT ACTIVITIES

	NO. OF COPIES
ANAMET LABORATORIES, 100 Industrial Hyw., San Carlos, CA 94070	
(Attn: Dr. R. Arnold).	1
ALCOA DEFENSE SYSTEMS CORP., 16761 Via delCampo Court, San Diego, CA 92127	
(Attn: D. Myers).	1
AVCO, Specialty Materials Div., 2 Industrial Avenue, Lowell, MA 01851	
(Attn: Mr. W. F. Grant).	1
BATTELLE COLUMBUS LABORATORIES, Metals and Ceramics Information Center 505 King Avenue, Columbus, OH 43201.	1
BEECH AIRCRAFT CORP., 4130 Linden Avenue, Dayton, OH 45432	
(Attn: M. B. Goetz).	1
BELL AEROSPACE COMPANY, Buffalo, NY 14240	
(Attn: F. M. Anthony, Zone I-85).	1
BELL HELICOPTER CO., Fort Worth, TX 76101	
(Attn: M. K. Stevenson).	1
BENDIX PRODUCTS, Aerospace Division, South Bend, IN 46619	
(Attn: R. V. Cervelli).	1
BOEING CO., P. O. Box 3707, Seattle, WA 98124	
(Attn: J. McCarty, J. Quinliven, and Dr. R. June). . .	3
BOEING CO., Vertol Division, P.O. Box 16858, Philadelphia, PA 19143	
(Attn: R. L. Pinckney).	1
(Attn: D. Hart).	1
(Attn: C. Albrecht).	1
BOEING CO., Wichita, KS 67277-7730.	1
(Attn: J. Avery).	1
(Attn: R. Waner).	1
CABOT CORPORATION, Billerica Research Center, Billerica, MA 01821.	1
DEPARTMENT OF TRANSPORTATION, Kendall Square, Cambridge, MA 02142.	1
(Attn: Dr. Ping Tong, DTS 76, TSC).	1
DREXEL UNIVERSITY, Philadelphia, PA 19104	
(Attn: Dr. P. C. Chou).	1
(Attn: Dr. A. S. D. Wang).	1
E. I. DuPONT COMPANY, Textile Fibers Department, Chestnut Run Location CR701, Wilmington, DE 19898	
(Attn: V. L. Bertarelli).	1
FAIRCHILD REPUBLIC CO., Farmingdale, L.I., NY 11735	
(Attn: Mr. Frank Costa).	1
GEORGIA INSTITUTE OF TECHNOLOGY, Atlanta, GA 30332	
(Attn: (L. Rehfield)).	1
GENERAL DYNAMICS/CONVAIR, San Diego, CA 92138	
(Attn: Dr. R. Dunbar).	1
GENERAL DYNAMICS, Fort Worth Division, PO Box 748, Fort Worth, TX 76101	
(Attn: J. A. Fant).	1
(Attn: Composite Structures Eng. Dept.).	1

DISTRIBUTION LIST

NON-GOVERNMENT ACTIVITIES (continued)

	NO. OF COPIES
NORTHROP AIRCRAFT CORP., One Northrop Avenue, Hawthorne, CA 90250 (Attn: Dr. M. Ratwani, B. Butler and R. Whitehead). . .	3
PURDUE UNIVERSITY, School of Aeronautics and Astronautics, West Lafayette, IN 47907 (Attn: Dr. C. T. Sun).	1
PROTOTYPE DEVELOPMENT ASSOCIATES, INC., 1560 Brookhollow Drive Santa Ana, CA 92705 (Attn: E. L. Stanton).	1
ROCKWELL INTERNATIONAL, Columbus, OH 43216 (Attn: M. Schweiger).	1
ROCKWELL INTERNATIONAL, Los Angeles, CA 90009 (Attn: Dr. Lackman).	1
(Attn: W. O'Brien).	1
ROCKWELL INTERNATIONAL, Tulsa, OK 74151 (Attn: F. Kaufman).	1
ROHR CORP., Riverside, CA 92503 (Attn: Dr. F. Riel).	1
SIKORSKY AIRCRAFT, Stratford, CT 06622 (Attn: S. Garbo).	1
J. P. STEVENS & CO., INC., New York, NY 10036 (Attn: H. I. Shulock).	1
TELEDYNE RYAN AERONAUTICAL CO., San Diego, CA 92138 (Attn: R. Long).	1
UNIVERSITY OF DAYTON RESEARCH INSTITUTE, 300 College Park Avenue, Dayton, OH 45469 (Attn: Dr. J. Gallagher).	1
UNIVERSITY OF DELAWARE, Mechanics & Aerospace Eng. Dept., Evans Hall, Newark, DE 19711 (Attn: Dr. R. B. Pipes, Dr. J. R. Vinson and Dr. D.Wilkins .	3
UNIVERSITY OF OKLAHOMA, Norman, OK 73019 (Attn: Dr. C. W. Bert, School of AMNE).	1
UNIVERSITY OF WYOMING, Laramie, WY 82071 (Attn: Dr. D. Adams).	1
VILLANOVA UNIVERSITY, Villanova, PA 19085 (Attn: Dr. P. V. McLaughlin).	1
VIRGINIA POLYTECHNIC INSTITUTE, Blacksburg, VA 24061 (Attn: Dr. K. Reifsnider).	1
WASHINGTON UNIVERSITY, School of Engineering and Applied Science, Materials Research Laboratory, Campus Box 1087, St. Louis, MO 63130 (Attn: T. Hahn).	1

DISTRIBUTION LIST

NON-GOVERNMENT ACTIVITIES (continued)

	NO. OF COPIES
NORTHROP AIRCRAFT CORP., One Northrop Avenue, Hawthorne, CA 90250 (Attn: Dr. M. Ratwani, B. Butler and R. Whitehead). . .	3
PURDUE UNIVERSITY, School of Aeronautics and Astronautics, West Lafayette, IN 47907 (Attn: Dr. C. T. Sun).	1
PROTOTYPE DEVELOPMENT ASSOCIATES, INC., 1560 Brookhollow Drive Santa Ana, CA 92705 (Attn: E. L. Stanton).	1
ROCKWELL INTERNATIONAL, Columbus, OH 43216 (Attn: M. Schweiger).	1
ROCKWELL INTERNATIONAL, Los Angeles, CA 90009 (Attn: Dr. Lackman).	1
(Attn: W. O'Brien).	1
ROCKWELL INTERNATIONAL, Tulsa, OK 74151 (Attn: F. Kaufman).	1
ROHR CORP., Riverside, CA 92503 (Attn: Dr. F. Riel).	1
SIKORSKY AIRCRAFT, Stratford, CT 06622 (Attn: S. Garbo).	1
J. P. STEVENS & CO., INC., New York, NY 10036 (Attn: H. I. Shulock).	1
TELEDYNE RYAN AERONAUTICAL CO., San Diego, CA 92138 (Attn: R. Long).	1
UNIVERSITY OF DAYTON RESEARCH INSTITUTE, 300 College Park Avenue, Dayton, OH 45469 (Attn: Dr. J. Gallagher).	1
UNIVERSITY OF DELAWARE, Mechanics & Aerospace Eng. Dept., Evans Hall, Newark, DE 19711 (Attn: Dr. R. B. Pipes, Dr. J. R. Vinson and Dr. D.Wilkins .	3
UNIVERSITY OF OKLAHOMA, Norman, OK 73019 (Attn: Dr. C. W. Bert, School of AMNE).	1
UNIVERSITY OF WYOMING, Laramie, WY 82071 (Attn: Dr. D. Adams).	1
VILLANOVA UNIVERSITY, Villanova, PA 19085 (Attn: Dr. P. V. McLaughlin).	1
VIRGINIA POLYTECHNIC INSTITUTE, Blacksburg, VA 24061 (Attn: Dr. K. Reifsnider).	1
WASHINGTON UNIVERSITY, School of Engineering and Applied Science, Materials Research Laboratory, Campus Box 1087, St. Louis, MO 63130 (Attn: T. Hahn).	1

END

DATE

FILMED

APRIL

1988

DTIC